ALMA MATER STUDIORUM

UNIVERSITY OF BOLOGNA

**PhD in**

**MATHEMATICS**

**XXVII Cycle**

Disciplinary Scientific Sector: MAT/07

# Predictability in Social Science, The statistical mechanics approach.

**PhD Thesis submitted by: Seyedalireza Seyedi**

**PhD Coordinator:** **Prof.** **Giovanna Citti**

**Supervisor:** **Prof.** **Pierluigi Contucci**

**Final Exam year 2014**

# Table of Contents

# INTRODUCTION

In recent years, there has been considerable effort to apply ideas and techniques from statistical physics to other areas of science such as economic, finance, social science and biology. Explaining the social phase transition, modeling the collective animal behavior (like natural flocks of birds), and predicting the financial market trend and crisis are some well-known examples of these efforts (see Mantegna and Stanley 1999; Castellano et al. 2000; Bouchaud and Potters 2004; Levy 2005; Ballerini et al. 2008; Contucci et al. 2008; Stanley 2008; Bialek et al. 2012). In particular, such applications have been used recently to study immigration phenomenon (Contucci and Giardina 2008; Barra et al 2014). It is notable to say that a particular political challenge of immigration is immigrant integration because the immigrant population changes a society's population composition and also immigration and integration of immigrants is considered key in building a competitive and sustainable economy in the world's leading economic regions (Niessen and Huddleston 2010; Castles and Miller 2009; European Commission 2011; IOM 2011; European Commission 2014; European Commission 2010; European Council 2010; Giovagnoli 2011; Canada Government 2012). For these reasons, the demand for political intervention rise accordingly (Castles and Miller 2009; European Commission 2011; IOM 2011; European Commission 2014), and consequently policies addressing the welcoming and the integration of immigrants are increasingly at the top of the policy agenda when policy makers try to tap the potential benefits of immigration (European Council 2010; Giovagnoli 2011; Canada Government 2012). Thus, policymakers need to be able to rely on theories and works generating strong predictions of the integration process, preferably early on in the immigration cycle (Contucci and Giardina 2008; Barra and Contucci 2010). A recent evidence, in a study inspired by ideas and techniques from statistical physics who make use of the concept of particle interaction have shown that while classical integration quantifiers, such as permanent and temporary jobs given to immigrants, grow proportionally to the immigrant density, newborns from mixed couples (one immigrant and one native parent) and mixed marriages have a growth law proportional to the square root of the immigrant density (Barra et al 2014). The sociological theory used to identify and explain such differences draws on the Weberian notion of *social action* (Weber 1978). When a choice with integration implications is induced by *social action* (social consensus and/or interaction) rather than by independent decisions (decision unaffected by others decisions) the square root growth law of the integration quantifier predominates over the linear growth law. This nontrivial explanation of the integration process is a useful tool if the goal is to formulate policies that regulate immigration. In what follows we perform a formal test of the theory's forecast potential with the aim to facilitate political decision making in the area of immigration and immigrant integration. Our objectives are twofold: 1) for a given integration context, we set out to forecast which mechanism – social or individual – predominate in the integration process, and 2) once the growth law is determined, we establish if and to what extent the methodological framework lends itself also to forecast immigrant integration and generate precise and robust estimates of integration levels across time.

To do so, the thesis is organized as follows: The first chapter provides a review of the literatures on mean field models which are the basis of formation of Barra et al's theoretical approach. Those mean filed models that we study here are: "Curie-Weiss", "Bipartite Curie-Weiss", and "Monomer-Dimer with attractive interaction" models. The literatures include explaining the computation of thermodynamic limit of the pressure for each model to achieve their consistency equations. One can say here is that the technique used to solve Curie-Weiss models is the same as one developed in the wider study of the mean field spin glasses by Guerra (2005) and also the solution of the monomer-dimer one is obtained with the help of Heilmann-Lieb method for the pure hard-core interacting case (Heilmann and Lieb 1970; Heilmann and Lieb 1972). To be more effective in this task, in the second chapter we study the nature of the phase transition that occurs in each defined model with detailed plots of critical surface around their critical point. Depending on the type of each consistency equation, this numerical study is done by application of a suitable numerical root-finding for computing zeros of the equation in order to build the shape of phase transition surface:

*Brent-Dekker* method for one population case (Brent 1973; Dekker 1969) and *trust-region* method for bipartite one (Conn et al 2000). The last chapter is dedicated to show an application of those models in socio-economic problems. More precisely, this chapter presents results on the forecasting ability of a recent finding by Barra et al (2014) where the behavior of integration quantifiers was analyzed and investigated with the mathematical models introduced in the first chapter. We show that not only such a method is able to identify the social mechanism that drives a particular integration process, but it also provides correct quantitative forecast of the process. By reducing uncertainties on how integration phenomena emerge and how they are likely to develop in response to increased migration levels in the future, our work provides a simple and effective tool for policy makers.

# THE MEAN-FIELD MODELS

In statistical mechanics, solving the physical models plays an important role in the study of phase transitions phenomena. However, achieving this purpose is quite hard to follow, but in some limited cases, in order to understand the basic features of such phenomena, the exact solution can be derived by using inventive methods such as mean-field theory. In those cases, the theoretical method tries to simplify the complex model to simpler one whose global behavior can be studied much easier, with the help of explicit and exact computations. Such global behavior can be then used to show which type of properties can be anticipated from the original model. This chapter explains how the theory applies for some well-known ferromagnetic models (i.e. the *Curie-Weiss* cases and *Monomer-Dimer* system with attractive interactions) in order to study their critical behaviors - so that such studies leads to be more effective in the next two chapters.

## The Curie-Weiss Model

The idea of mean field theory first appeared in the work of Pierre Curie and Pierre Weiss when they explained a simple classical system that exhibits phase transition (Curie 1895; Weiss 1907). Pierre Weiss explained a simple classical system that exhibits phase transition based on the experimental observations carried out by Pierre Curie. Weiss studied the behavior of a set of magnetic moments interacting with their nearest neighbors. Their model, so-called *Curie-Weiss* model, as an exactly solvable ferromagnetic model helps us to study the properties of the thermodynamic functions very close to the critical temperature. In this section, we discuss the properties of the model in a rather detailed way including thermodynamic limit computation, and getting the consistency equation.

## The Model

To define the ferromagnetic *Curie-Weiss* model let us first consider an interacting system of $N$ particles whose Hamiltonian is given by:

$$H_N(\sigma) = -\frac{J}{2N}\sum_{i,j=1}^{N}\sigma_i\sigma_j - h\sum_{i=1}^{N}\sigma_i, \tag{1.1}$$

where $\sigma_i = \pm 1$ is the spin of the particle $i$, the positive parameter $J$ is interacting constant, and $h$ indicates the value of the external field. In addition, let us specify the magnetization of the configuration $\sigma$ as:

$$m_N(\sigma) = \frac{1}{N}\sum_{i=1}^{N}\sigma_i. \tag{1.2}$$

Hence, the Hamiltonian per particle can be rewritten as:

$$H_N(\sigma) = -N(g(m_N(\sigma))), \tag{1.3}$$

where

$$g\big(m_N(\sigma)\big) = \frac{J}{2}m_N(\sigma)^2 + hm_N(\sigma). \tag{1.4}$$

Furthermore, for a generic observable $f(\sigma)$, we define the Gibbs state as:

$$\omega_N(f) = \frac{\sum_\sigma f(\sigma)exp(-H_N(\sigma))}{Z_N},$$

where $Z_N$ indicates the partition function of the system:

$$Z_N = \sum_\sigma exp(-H_N(\sigma)). \tag{1.5}$$

Thus, all these definitions allow us to obtain the pressure function per particle associated to the thermodynamic system by:

$$p_N = \frac{1}{N}log\sum_\sigma exp(-H_N(\sigma)). \tag{1.6}$$

Moreover, one can say here is that the pressure (1.6) generates the mean with respect to the Gibbs state $\omega_N$ of the magnetization (1.2) as follow:

$$\langle m_N(\sigma)\rangle = \frac{\partial p_N}{\partial h}. \tag{1.7}$$

## The Thermodynamic Limit

In statistical physics, the thermodynamic limit is a mathematical technique that denotes the limiting behavior of a physical system consisting of many particles. Many features of the macroscopic physical systems only emerge in this limit such as phase transitions and other critical phenomena. The question of existence of these thermodynamical limits poses lots of mathematical problems and consequently response to this question is rather complicated. In this section, we suggest a simple strategy based on the interpolation method to demonstrate the existence of the thermodynamic for the ferromagnetic Curie-Weiss model. Our strategy is independent from the exact solution and relies on the existence theory proved for mean field models by Bianchi et al (2004). For doing this, let us first consider an interacting system of $N$ particles defined above and next divide it into two subsets $P_1$ and $P_2$ with $|P_1| = N_1$ and $|P_2| = N_2$ such that $N_1 + N_2 = N$. Therefore, in order to show that the model admits the thermodynamic limit of the pressure, we only need to express and prove the following proposition:

**Proposition 1.1.** Let $J \geq 0$, $h \in \mathbb{R}$. The pressure per particle of the mean field ferromagnetic *Curie-Weiss* model defined by Hamiltonian (1.3) admits the thermodynamic limit:

$$\lim_{N\to\infty} p_N(J,h) = p.$$

***Proof.*** Bianchi et al (2004) proved that for any mean-field model defined by its Hamiltonian $H_N$ and its relevant equilibrium state $\omega_N$, the thermodynamic limit of the model exists in the sense that: $\lim_{N\to\infty} p_N = p$; if the condition

$$\omega_N(H_N) \geq \omega_N(H_{N_1} + H_{N_2}) \tag{1.8}$$

is verified for every partition of the set $\{1, \dots, N\}$ into $\{1, 2, \dots, N_1\}$ and $\{\underbrace{N_1 + 1, \dots, N}_{N_2}\}$ with $N_1 + N_2 = N$ and $H_{N_1} = H_{N_1}(\sigma_1, \dots, \sigma_{N_1})$, $H_{N_2} = H_{N_2}(\sigma_{N_1+1}, \dots, \sigma_N)$. Hence, we can define the following partial magnetizations associated with the subsets $P_1$ and $P_2$ for the given mean field ferromagnetic *Curie-Weiss* model:

$$m_{N_1}(\sigma) = \frac{1}{N_1}\sum_{i=1}^{N_1}\sigma_i \tag{1.9}$$

$$m_{N_2}(\sigma) = \frac{1}{N_2}\sum_{i=N_1+1}^{N}\sigma_i \tag{1.10}$$

Therefore, we have the following equation:

$$m_N(\sigma) = \frac{N_1}{N}m_{N_1}(\sigma) + \frac{N_2}{N}m_{N_2}(\sigma),$$

so that

$$H_N - H_{N_1} - H_{N_2} = -N\frac{J}{2}(m_N^2(\sigma) - \frac{N_1}{N}m_{N_1}^2(\sigma) - \frac{N_2}{N}m_{N_2}^2(\sigma)) \geq 0 \tag{1.11}$$

and from (1.11), we get:

$$\omega_N(H_N - H_{N_1} - H_{N_2}) = -N\omega_N(g(m_N(\sigma)) - \frac{N_1}{N}g(m_{N_1}(\sigma)) - \frac{N_2}{N}g(m_{N_2}(\sigma))) \tag{1.12}$$

such that the equation (1.12) and the convexity of the function $g$ imply that

$$\omega_N(H_N - H_{N_1} - H_{N_2}) \geq 0.$$

Thus, the condition (1.8) is verified and the proof is completed ■.

## The Solution

It is well-known that computing the upper and lower bounds for the thermodynamic limit of the pressure leads to obtain the exact solution of statistical-mechanics models. Relying on this procedure, we so begin, following (Contucci and Gallo 2008), by dividing the space of the configuration into a microstates partition of equal magnetization. Since the system has $N$ spins, the magnetization can explicitly take $N+1$ values. That is to say, such values can be shown as the elements of the set:

$$\Sigma = \left\{-1, -1 + \frac{1}{2N}, \dots, 1 - \frac{1}{2N}, 1\right\}. \tag{1.13}$$

By defining the Kronecker delta $\delta_{m,\widetilde{m}}$, for every $m(\sigma)$ we have $\sum_{\widetilde{m}\in\Sigma}\delta_{m,\widetilde{m}} = 1$, and by setting it inside the partition function (1.5) we can obtain:

$$Z_N = \sum_\sigma \exp\left\{N\left(\frac{J}{2}m_N^2 + hm_N\right)\right\}$$

$$= \sum_\sigma \sum_{\widetilde{m}\in\Sigma} \delta_{m_N,\widetilde{m}} exp\left\{N(\frac{J}{2}m_N^2 + hm_N)\right\}.$$

At this point, one can see is that the delta function forces the equality $m_N = \widetilde{m}$ inside the sum.

Thus, the equality $m_N^2 = 2m_N\widetilde{m} - \widetilde{m}^2$ can be used in the sum:

$$Z_N = \sum_\sigma \sum_{\widetilde{m}\in\Sigma} \delta_{m_N,\widetilde{m}} exp\left\{N(\frac{J}{2}(2m_N\widetilde{m} - \widetilde{m}^2) + hm_N)\right\}.$$

To proceed, let us now omit the Kronecker delta by $\delta \leq 1$ so that:

$$Z_N \leq \sum_\sigma \sum_{\widetilde{m}\in\Sigma} exp\left\{N(\frac{J}{2}(2m_N\widetilde{m} - \widetilde{m}^2) + hm_N)\right\}.$$

We can exchange the order of the two summation symbols because both sums are finite:

$$Z_N \leq \sum_{\widetilde{m}\in\Sigma} \exp\left\{-N\frac{J}{2}\widetilde{m}^2\right\}. 2^N(\cosh(J\widetilde{m} + h))^N.$$

Clearly, the total number of summands is $N + 1$ therefore we have that

$$Z_N \leq (N+1)\sup_{\widetilde{m}} G(\widetilde{m}), \tag{1.14}$$

where $G(\widetilde{m}) = \exp\left\{-N\frac{J}{2}\widetilde{m}^2\right\}. 2^N(\cosh(J\widetilde{m} + h))^N$. Thus, we can obtain the following inequality:

$$p_N \leq \frac{1}{N}\ln((N+1)\sup_{\widetilde{m}} G(\widetilde{m})) \tag{1.15}$$

$$= \frac{1}{N}\ln(N+1) + \frac{1}{N}\sup_{\widetilde{m}} \ln(G(\widetilde{m})). \tag{1.16}$$

Since $\lim_{N\to\infty}\frac{1}{N}\ln(N+1) = 0$, we get:

$$\limsup_{N\to\infty} p_N \leq \sup_{\widetilde{m}} p_{upper}(\widetilde{m}) \tag{1.17}$$

where

$$p_{upper}(\widetilde{m}) = \ln 2 - \frac{J}{2}\widetilde{m}^2 + \ln(\cosh(J\widetilde{m} + h)) \tag{1.18}$$

In another side, to obtain the lower bound, it is enough to set the inequality $m_N^2 \geq 2m_N\widetilde{m} - \widetilde{m}^2$ into the partition function (1.5) and then we have that:

$$p_N(J,h) = \frac{1}{N}\ln Z_N = \frac{1}{N}\ln\sum_{\sigma}\exp\left\{N\left(\frac{J}{2}m_N^2 + hm_N\right)\right\}$$

$$\geq \frac{1}{N}\ln\sum_{\sigma}\exp\left\{N\left(Jm_N\widetilde{m} - \frac{J}{2}\widetilde{m}^2 + hm_N\right)\right\}$$

$$= \frac{1}{N}\ln\left(\exp\left\{-N\frac{J}{2}\widetilde{m}^2\right\}\sum_{\sigma}\exp\{N(Jm_N\widetilde{m} + hm_N)\}\right)$$

$$= -\frac{J}{2}\widetilde{m}^2 + \frac{1}{N}\ln(2^N.\cosh(J\widetilde{m} + h)^N) = -\frac{J}{2}\widetilde{m}^2 + \ln 2 + \ln(\cosh(J\widetilde{m} + h))$$

Now we can state the lower bound as follow:

$$p_N(J,h) \geq \sup_{-1\leq\widetilde{m}\leq 1} p_{lower}(\widetilde{m}) \tag{1.19}$$

where

$$p_{lower}(\widetilde{m}) = -\frac{J}{2}\widetilde{m}^2 + \ln 2 + \ln(\cosh(J\widetilde{m} + h)). \tag{1.20}$$

Finally, we can summarize these results in the following theorem:

**Theorem 1.1.** Let $J \geq 0$ and $h \in \mathbb{R}$. For any given Hamiltonian in the form of (1.3), the thermodynamic limit exists in the sense:

$$\lim_{N\to\infty} p_N(J,h) = p$$

where $p$ can be expressed as $p = \sup_{\widetilde{m}} p_{lower}(\widetilde{m})$ or $p = \sup_{\widetilde{m}} p_{upper}(\widetilde{m})$. Accordingly, the limit of the pressure as $N \to \infty$ is obtained by maximization of $p_{lower}(\widetilde{m})$ or $p_{upper}(\widetilde{m})$. Thus, differentiating $p_{lower}(\widetilde{m})$ (or $p_{upper}(\widetilde{m})$) with respect to $\widetilde{m}$ leads to obtain the consistency equation of the model as follow:

$$\frac{\partial p_{lower}(\widetilde{m})}{\partial\widetilde{m}} = 0$$

$$\Rightarrow \frac{\partial p_{lower}(\widetilde{m})}{\partial\widetilde{m}} = -J\widetilde{m} + J\frac{\sinh(J\widetilde{m}+h)}{\cosh(J\widetilde{m}+h)} = -J\widetilde{m} + Jtanh(J\widetilde{m} + h) = 0 \tag{1.21}$$

$$\Rightarrow \widetilde{m} = tanh(J\widetilde{m} + h) \tag{1.22}$$

# The Bipartite Curie-Weiss Model

This section explains the two populations mean field model as a generalization of the ferromagnetic Curie-Weiss model. In recent decades, there have been several attempts to introduce bipartite mean field models for description of physical phenomena such as the phase transition state of metamagnets, structure of the antiferromagnetic system, and the loss of gibbsianness for a lattice system where defined by Glauber dynamic (Motizuki 1959; Kincaid and Cohen 1975; Galam et al 1998; Kulske and Le Ny 2007). In particular, such models have been recently applied for describing the large scale behavior of some socio-economic systems when interactions exist in the form of imitative decisions (Contucci and Ghirlanda 2008). Additionally, the non-interacting ones also were used in the basic idea of building the discrete choice theory by McFadden to predict the choice of some socio-economic agents (McFadden 2001). The interacting case of such theory was first suggested by Contucci and Ghirlanda (2008) and then extended by Barra et al (2014) to describe the integration of immigrants mechanism. This section first explains the existence of the thermodynamic limit of *bipartite Curie-Weiss* model proved by Gallo and Contucci (2008) in which an asymptotic sub-addittivity method were used analogous to one developed by Guerra (2005) in order to derive identities for the overlap distributions in the Sherrington and Kirkpatrick model. Following Fedele (2011), we then proceed by computing the self-consistency equation of the bipartite model using the technique proposed by Talagrand (2003).

## The Model

Consider a set of $N$ spin variables, and assume the partition of the set which is defined by two subsets of size $N_1$ and $N_2$ respectively with the term $N_1 + N_2 = N$. Now suppose that while the variable's label of the first subset is $\sigma_i, i = 1, \dots, N_1$, the spins of the second one are in form of $\sigma_j, j = N_1 + 1, \dots, N$. The particles interact via the Hamiltonian

$$H_N(\sigma) = -\frac{1}{2N}\sum_{i,j=1}^{N} J_{ij}\sigma_i\sigma_j - \sum_{i=1}^{N} h_i\sigma_i, \tag{1.23}$$

where $\sigma_i = \pm 1$ represents the spin of the particle $i$. Parameter $J_{ij}$ tunes the mutual interaction between particles $i$ and $j$ which specifies according to the following matrix:

$$\begin{array}{c c} & \begin{array}{cc} \overbrace{\phantom{J_{11}}}^{N_1} & \overbrace{\phantom{J_{12}}}^{N_2} \end{array} \\ \begin{array}{c} N_1 \{ \\ N_2 \{ \end{array} & \left[\begin{array}{c|c} \boldsymbol{J_{11}} & \boldsymbol{J_{12}} \\ \hline \boldsymbol{J_{12}} & \boldsymbol{J_{22}} \end{array}\right] \end{array}$$

where the blocks $\boldsymbol{J_{11}}$ and $\boldsymbol{J_{22}}$ indicate the interaction between the particles within each of the two subsets and $\boldsymbol{J_{12}}$ shows the interaction between the particles of different subsets. In the blocks, we assume all the values $J_{11}$, $J_{22}$, and $J_{12}$ are positive. Similarly, the vector magnetic field $h_i$ is assigned with values $h_1$and $h_2$ depending on the subsets the particles belong to and specified by:

$$\begin{array}{c c} \begin{array}{c} N_1 \{ \\ N_2 \{ \end{array} & \left[\begin{array}{c} \boldsymbol{h_1} \\ \hline \boldsymbol{h_2} \end{array}\right] \end{array}$$

Assume the joint distribution of a spin configuration $\sigma = (\sigma_1, \dots, \sigma_N)$ is given by the Boltzmann-Gibbs measure as follow:

$$P_{N,\boldsymbol{J},\boldsymbol{h}}\{\sigma\} = \frac{\exp(-H_N(\boldsymbol{\sigma}))}{Z_N(\mathbf{J},\mathbf{h})} \prod_{i=1}^{N} d\rho(\sigma_i) \tag{1.24}$$

where

$$Z_N(\mathbf{J},\mathbf{h}) = \int_{\mathbb{R}^N} \exp(-H_N(\boldsymbol{\sigma})) \prod_{i=1}^{N} d\rho(\sigma_i) \tag{1.25}$$

is the partition function of the system and the measure $\rho$ is:

$$\rho = \frac{1}{2}(\delta(x-1) + \delta(x+1)),$$

where the delta Dirac function $\delta(x - x_0)$ with $x_0 \in \mathbb{R}$ indicates the unit point mass with support at $x_0$. By definition of $\rho$ each spin can take only one of the values $\{+1, -1\}$. Now assume that the respective magnetizations of the two subsets are:

$$m_1(\sigma) = \frac{1}{N_1}\sum_{i=1}^{N_1} \sigma_i$$

$$m_2(\sigma) = \frac{1}{N_2}\sum_{i=N_1+1}^{N} \sigma_i$$

We name the relative size of the two subsets $\alpha_1 = \frac{N_1}{N}$ and $\alpha_2 = \frac{N_2}{N}$. Henceforth, assume that $\alpha_1 = \alpha$ and $\alpha_2 = 1-\alpha$ where $\alpha \in [0,1]$. The entire definitions together permits to simplify the Hamiltonian function in the following form:

$$\frac{H_N(\sigma)}{N} = -\frac{1}{2}[\alpha J_{11}m_1^2 + 2\alpha(1-\alpha)J_{12}m_1m_2 + (1-\alpha)J_{22}m_2^2] - \alpha h_1m_1 - (1-\alpha)h_2m_2 \quad (1.26)$$

Therefore, the mean field form of (1.26) can be written as:

$$H_N = -Ng(m_1, m_2) \quad (1.27)$$

with a convex bounded function

$g(m_1, m_2) = \frac{1}{2}[\alpha J_{11}m_1^2 + 2\alpha(1-\alpha)J_{12}m_1m_2 + (1-\alpha)J_{22}m_2^2] - \alpha h_1m_1 - (1-\alpha)h_2m_2.$

By defining $\mathbf{J} = \begin{bmatrix} J_{11} & J_{12} \\ J_{12} & J_{22} \end{bmatrix}$, $\mathbf{h} = \begin{bmatrix} h_1 \\ h_2 \end{bmatrix}$, the function $g$ can be written in a compact way as

$$g(\mathbf{m}) = \frac{1}{2}\langle \tilde{\mathbf{J}}\mathbf{m}, \mathbf{m}\rangle + \langle \tilde{\mathbf{h}}, \mathbf{m}\rangle \quad (1.28)$$

where the matrix $\tilde{\mathbf{J}} = \mathbf{D}_\alpha\mathbf{D}_\alpha\mathbf{J}\mathbf{D}_\alpha\mathbf{D}_\alpha$, the vector $\tilde{\mathbf{h}} = \mathbf{D}_\alpha\mathbf{D}_\alpha\mathbf{h}$, the matrix $\mathbf{D}_\alpha = diag\{\sqrt{\alpha}, \sqrt{1-\alpha}\}$, and $\langle . \rangle$ is scalar product. Indeed, since we need to find the value of $\langle m_N(\sigma)\rangle$ and foremost we know very well that the main observable here is the average of the spin configuration $m_N(\sigma)$, we consider the pressure function

$$p_N = \frac{1}{N} log \sum_\sigma exp(-H_N(\sigma)) \quad (1.29)$$

which is capable of generating the averages of the magnetization with respect to the Gibbs state as:

$$\langle m_N(\sigma)\rangle = \alpha\frac{\partial p_N}{\partial h_1} + (1-\alpha)\frac{\partial p_N}{\partial h_2} \quad (1.30)$$

## The Thermodynamic Limit

To show that the thermodynamic limit of the model exists, we state and prove the following theorem.

**Theorem 1.2.** Let $J_{11}, J_{22}, J_{12} \geq 0$, $h_1, h_2 \in \mathbb{R}$, and $\alpha \in [0,1]$. The pressure per particle of the mean field ferromagnetic model defined by Hamiltonian (1.24) admits the thermodynamic limit:

$$\lim_{N\to\infty} p_N(J,h) = p.$$

***Proof.*** Let us first write our Hamiltonian $H_N$ in the form

$$H_N = H_N^{(1)} + H_N^{(12)} + H_N^{(2)} \tag{1.31}$$

where $H_N^{(1)} = \frac{1}{N} J_{11} \sum_{i,j=1,\dots,N_1} \xi_i \xi_j$, $H_N^{(2)} = \frac{1}{N} J_{22} \sum_{i,j=1,\dots,N_2} \eta_i \eta_j$, $H_N^{(12)} = \frac{1}{N} J_{12} \sum_{\substack{i=1,\dots,N_1 \\ j=1,\dots,N_2}} \xi_i \eta_j$ with $\xi = \pm 1$ and $\eta = \pm 1$. We then proceed by defining the model with a working Hamiltonian as

$$\widetilde{H}_N = \widetilde{H}_N^{(1)} + \widetilde{H}_N^{(12)} + \widetilde{H}_N^{(2)} \tag{1.32}$$

where

$$\widetilde{H}_N^{(1)} = \alpha J_{11} \frac{1}{\alpha N - 1} \sum_{i \neq j=1,\dots,N_1} \xi_i \xi_j,$$

$$\widetilde{H}_N^{(2)} = (1-\alpha) J_{22} \frac{1}{(1-\alpha)N - 1} \sum_{i \neq j=1,\dots,N_2} \eta_i \eta_j,$$

and

$$\widetilde{H}_N^{(12)} = \frac{1}{N} J_{12} \sum_{\substack{i=1,\dots,N_1 \\ j=1,\dots,N_2}} \xi_i \eta_j.$$

From definition $H_N^{(1)}$ and using $\alpha = \frac{N_1}{N}$ we have that

$$H_N^{(1)} = \frac{N_1 - 1}{N} J_{11} \frac{1}{N_1 - 1} \sum_{i \neq j=1,\dots,N_1} \xi_i \xi_j + \frac{1}{N} J_{11} \sum_{i=1,\dots,N_1} \xi_i \xi_j$$

$$= \frac{\alpha N - 1}{\alpha N} \alpha J_{11} \frac{1}{\alpha N - 1} \sum_{i \neq j=1,\dots,N_1} \xi_i \xi_j + \alpha J_{11}$$

$$= \underbrace{\alpha J_{11} \frac{1}{\alpha N - 1} \sum_{i \neq j=1,\dots,N_1} \xi_i \xi_j}_{\widetilde{H}_N^{(1)}} + \underbrace{\left(-\alpha J_{11} \frac{1}{\alpha N(\alpha N - 1)} \sum_{i \neq j=1,\dots,N_1} \xi_i \xi_j + \alpha J_{11}\right)}_{O(1)},$$

$$\Rightarrow H_N^{(1)} = \widetilde{H}_N^{(1)} + O(1).$$

Similarly we can repeat the same computation for $H_N^{(2)}$ and $H_N^{(12)}$ in terms of $\widetilde{H}_N^{(2)}$ and $\widetilde{H}_N^{(12)}$ and it follows that

$$H_N = \widetilde{H}_N + O(1). \tag{1.33}$$

It implies that

$$\lim_{N\to\infty} \frac{H_N}{N} = \lim_{N\to\infty} \frac{\widetilde{H}_N}{N}. \tag{1.34}$$

Using the following proposition one has that the both models $H_N$ and $\widetilde{H}_N$ have the same thermodynamic limit (if any).

**Proposition 1.2.** Define the Hamiltonian $H_N$, a bounded convex function $g_N = \frac{H_N}{N}$, partition function $Z_N$, and the pressure $p_N$ for our mean field model and in the same way $\widetilde{H}_N$, $\tilde{g}_N = \frac{\widetilde{H}_N}{N}$, $\tilde{Z}_N$ and $\tilde{p}_N$. If

$$k_N = \|g_N - \tilde{g}_N\| = \sup_{\sigma\in\{-1,+1\}^N} \{|g_N(\sigma) - \tilde{g}_N(\sigma)|\} < \infty$$

then

$$|p_N - \tilde{p}_N| \leq \|g_N - \tilde{g}_N\|.$$

*Proof of proposition.*

$$p_N - \tilde{p}_N = \frac{1}{N}\ln(Z_N) - \frac{1}{N}\ln(\tilde{Z}_N) = \frac{1}{N}\ln(\frac{Z_N}{\tilde{Z}_N})$$

$$= \frac{1}{N}\ln(\frac{\sum_\sigma \exp\left(-H_N(\sigma)\right)}{\sum_\sigma \exp\left(-\widetilde{H}_N(\sigma)\right)}) \leq \frac{1}{N}\ln(\frac{\sum_\sigma \exp\left(-H_N(\sigma)\right)}{\sum_\sigma \exp(-N(g_N(\sigma) + k_N))})$$

$$= \frac{1}{N}\ln\left(\frac{\sum_\sigma \exp\left(-H_N(\sigma)\right)}{\exp(-Nk_N)\sum_\sigma \exp\left(-N\left(g_N(\sigma)\right)\right)}\right) = \frac{1}{N}\ln(\exp(Nk_N)) = k_N = \|g_N - \tilde{g}_N\|$$

$$\Rightarrow p_N - \tilde{p}_N \leq \|g_N - \tilde{g}_N\|.$$

In analogous way, the inequality $\tilde{p}_N - p_N \leq \|g_N - \tilde{g}_N\|$ can be obtained and consequently the following is hold:

$$|p_N - \tilde{p}_N| \le \|g_N - \tilde{g}_N\|. \tag{1.35}$$

*End of proof of proposition.*

The proposition implies that

$$\lim_{N\to\infty}|p_N - \tilde{p}_N| \le \lim_{N\to\infty}\|g_N - \tilde{g}_N\| = 0. \tag{1.36}$$

From the definition $\widetilde{H}_N^{(1)}$ we have that

$$\omega_N\left(\widetilde{H}_N^{(1)}\right) = \omega_N(\alpha J_{11}\frac{1}{\alpha N-1}\sum_{i\neq j=1,\dots,N_1}\xi_i\xi_j) = \alpha J_{11}\frac{(\alpha N-1)\alpha N}{\alpha N-1}\omega_N(\xi_i\xi_j) = N\alpha^2 J_{11}\omega_N(\xi_i\xi_j).$$

In similar way, we can repeat the same computation for $\widetilde{H}_N^{(2)}$ and $\widetilde{H}_N^{(12)}$ in the state $\omega_N$. Those computations together state that $\omega_N\left(\widetilde{H}_N - \widetilde{H}_N^{(1)} - \widetilde{H}_N^{(2)}\right) = 0$ is hold for $N_1 + N_2 = N$ which verifies the condition (1.8). It implies the existence of thermodynamic limit for the model of $\widetilde{H}_N$, , and so for the model $H_N$. Hence, the proof of the theorem is completed.

## The Solution

A main approach to obtain the exact solution of a mean field model is to drive the upper and lower bounds for its thermodynamic limit of the pressure. Thus, in this bipartite case, for obtaining the solution, following Fedele (2011) , the upper and lower bounds can be driven through the technique proposed by Talagrand (2003). To do so, first, the partition function of the system with respect to the Hamiltonian (1.26) can be written as

$$Z_N(\mathbf{J},\mathbf{h}) = \frac{1}{2^N}\sum_{\boldsymbol{\sigma}\in\Omega_N}\exp(-H_N(\boldsymbol{\sigma})).$$

where the space $\Omega_N = \{+1,-1\}^N$ is the space of all possible configuration $\boldsymbol{\sigma}$. We introduce the configuration of the spins of the set $P_l$ with $\boldsymbol{\sigma}_l$ where $l = 1{,}2$ and accordingly we can define the notation

$$A_{\mu_l} = \mathrm{card}\left\{\boldsymbol{\sigma}_l \in \Omega_{N_l} \mid m_l(\boldsymbol{\sigma}) = \mu_l\right\} \tag{1.37}$$

Let us now consider the mean filed Hamiltonian (1.27) with the function $g$ which is given by (1.28). Thus, we can represent the partition function as

$$Z_N(\mathbf{J},\mathbf{h}) = \frac{1}{2^N}\sum_{\mu}\prod_{l=1}^{2} A_{\mu_l}\exp(N(\frac{1}{2}\langle\tilde{\mathbf{J}}\boldsymbol{\mu},\boldsymbol{\mu}\rangle + \langle\tilde{\mathbf{h}},\boldsymbol{\mu}\rangle))$$

where the sum extends over all the possible values of the random vector $(m_1(\boldsymbol{\sigma}), m_2(\boldsymbol{\sigma}))$.

The following lemma proved by Fedele (2011) leads to obtain the bounds that we are interested in.

**Lemma 1.1.** Consider the set $\Omega_N = \{+1,-1\}^{N_l}$ of all possible configuration $\boldsymbol{\sigma}_l$. Let $A_{\mu_l}$ be a positive number defined by (1.37) the following inequality holds

$$\frac{1}{C}\frac{2^{N_l}}{\sqrt{N_l}}\exp(-N_l\Xi(A_{\mu_l})) \le A_{\mu_l} \le 2^{N_l}\exp(-N_l\Xi(A_{\mu_l})) \tag{1.38}$$

where $C$ is a constant and

$$\Xi(\mathrm{x}) = \frac{1}{2}((1+\mathrm{x})\ln(1+\mathrm{x}) + (1-\mathrm{x})\ln(1-\mathrm{x})) \tag{1.39}$$

Using lemma 1.1 allows us to compute the upper and lower bounds for the partition function as

$$\frac{1}{C}\prod_{l=1}^{2}\frac{1}{\sqrt{N_l}}\exp(N\max_{\mu}\bar{f}(\mu)) \le Z_N(\mathbf{J},\mathbf{h}) \le \prod_{l=1}^{2}(N_l+1)\exp(N\max_{\mu}\bar{f}(\mu))$$

where

$$\bar{f}(m_1,m_2) = \frac{1}{2}\sum_{l,s=1}^{2}\alpha_l\alpha_s J_{ls}m_l m_s + \sum_{l=1}^{2}\alpha_l h_l m_l + \sum_{l=1}^{2}\alpha_l\,\Xi(m_l) \tag{1.40}$$

Accordingly, by taking the logarithm and dividing by $N$, we have the bounds for the pressure as

$$-\frac{1}{N}\left(\ln C + \frac{1}{2}\sum_{l=1}^{2}\ln(N_l)\right) + \max_{\boldsymbol{\mu}}\bar{f}(\boldsymbol{\mu}) \le p_N(\mathbf{J},\mathbf{h}) \le \frac{1}{N}(\sum_{l=1}^{2}\ln(N_l+1)) + \max_{\boldsymbol{\mu}}\bar{f}(\boldsymbol{\mu}).$$

i.e.

$$p_{lower} = \frac{1}{2}(J_{11}\alpha^2\mu_1^2 + 2J_{12}\alpha(1-\alpha)\mu_1\mu_2 + J_{22}(1-\alpha)^2\mu_2^2) + \alpha h_1\mu_1 + (1-\alpha)h_2\mu_2 +$$

$$\alpha\left(-\frac{1+\mu_1}{2}\ln\left(\frac{1+\mu_1}{2}\right) - \frac{1-\mu_1}{2}\ln\left(\frac{1-\mu_1}{2}\right)\right) + (1-\alpha)\left(-\frac{1+\mu_2}{2}\ln(\frac{1+\mu_2}{2}) - \frac{1-\mu_2}{2}\ln(\frac{1-\mu_2}{2})\right) \tag{1.41}$$

It follows that the limit of the pressure as $N \to \infty$ can be computed by maximizing the function $\bar{f}$. As a result, differentiating of $\bar{f}$ with respect to $m_1, m_2$ leads to obtain the self-consistency equation of the bipartite model as follow:

$$\begin{cases} m_1 = \tanh(\alpha J_{11} m_1 + (1-\alpha) J_{12} m_2 + h_1) \\ m_2 = \tanh(\alpha J_{12} m_1 + (1-\alpha) J_{22} m_2 + h_2) \end{cases} \tag{1.42}$$

As $\mathbf{J}$ is a positive define, another reliable way we can focus for obtaining the consistency equation is application of the Thompson method (Thompson 1988) when we compute the thermodynamic limit. Thus, recalling the mean-field Hamiltonian (1.27), its partition function (1.25) can be expressed as,

$$Z_N(\mathbf{J}, \mathbf{h}) = \int_{\mathbb{R}^2} \exp(N(\frac{1}{2}\langle \tilde{\mathbf{J}}\mathbf{m}, \mathbf{m}\rangle + \langle \tilde{\mathbf{h}}, \mathbf{m}\rangle)) d\nu_M(\mathbf{m})$$

where $\nu_M$ is the distribution of the random vector $(m_1(\boldsymbol{\sigma}), m_2(\boldsymbol{\sigma}))$ on $(\mathbb{R}^N, \prod_{i=1}^N d\rho(\sigma_i))$. Let us write the following identity which is valid for the positive define matrix $\mathbf{J}$:

$$\exp\left(\frac{N}{2}\langle \tilde{\mathbf{J}}\mathbf{m}, \mathbf{m}\rangle\right) = \sqrt{\frac{N\det\tilde{\mathbf{J}}}{(2\pi)^2}} \int_{\mathbb{R}^2} \exp(-\frac{N}{2}\langle \tilde{\mathbf{J}}\mathrm{x}, \mathrm{x}\rangle + N\langle \mathrm{x}, \mathbf{m}\rangle) d\mathrm{x}$$

Using the above identity allows us to rewrite the partition function as,

$$Z_N(\mathbf{J}, \mathbf{h}) = \sqrt{\frac{N\det\tilde{\mathbf{J}}}{(2\pi)^2}} \times \iint_{\mathbb{R}^4} \exp(N(-\frac{1}{2}\langle \tilde{\mathbf{J}}\mathrm{x}, \mathrm{x}\rangle + \langle \tilde{\mathbf{h}}, \mathbf{m}\rangle + \langle \tilde{\mathbf{J}}\mathrm{x}, \mathbf{m}\rangle))\, d\nu_M(\mathbf{m}) d\mathrm{x}$$

$$= \sqrt{\frac{N\det\tilde{\mathbf{J}}}{(2\pi)^2}} \times \int_{\mathbb{R}^2} \exp(N(-\frac{1}{2}\langle \tilde{\mathbf{J}}\mathrm{x}, \mathrm{x}\rangle)) \int_{\mathbb{R}^2} \exp(N(\langle \tilde{\mathbf{J}}\mathrm{x} + \tilde{\mathbf{J}}, \mathbf{m}\rangle))\, d\nu_M(\mathbf{m}) d\mathrm{x}$$

and since we have:

$$\int_{\mathbb{R}^2} \exp(N(\langle \tilde{\mathbf{J}}\mathrm{x} + \tilde{\mathbf{J}}, \mathbf{m}\rangle))\, d\nu_M =$$

$$= \int_{\mathbb{R}^N} \exp(\sum_{l=1}^{2} \alpha_l \sum_{i\in P_l} \sigma_i \, (\sum_{s=1}^{2} \alpha_s J_{ls} x_s + h_l)) \prod_{i\in P_l} d\rho(\sigma_i)$$

$$= \prod_{l=1}^{2} \prod_{i\in P_l} \int_{\mathbb{R}} \exp(\alpha_l \sigma_i (\sum_{s=1}^{2} \alpha_s J_{ls} x_s + h_l))\, d\rho(\sigma_i)$$

By summing over the spins we can reformulate the partition function as,

$$Z_N(\mathbf{J},\mathbf{h}) = \sqrt{\frac{N\det\tilde{\mathbf{J}}}{(2\pi)^2}} \times \int_{\mathbb{R}^2} \exp(N(f(\mathrm{x})))\, d\mathrm{x}$$

where

$$f(x_1,x_2) = -\frac{1}{2}\sum_{l,s=1}^{2} \alpha_l\alpha_s J_{ls}x_l x_s + \sum_{l=1}^{2} \alpha_l \ln(\cosh(\sum_{s=1}^{2} \alpha_l J_{ls}x_s + h_l)) \tag{1.43}$$

Proposition 2.2.2 introduced and proved by Fedele 2011 states that for a given function (1.43) associated to a model defined by the Hamiltonian (1.27), if the reduced interaction matrix $J$ is positive define and if $\boldsymbol{\mu}$ be a global maximum of the function $f$, then

$$\lim_{N\to\infty} \frac{1}{N} \ln\left(\exp\left(Nf(\mathrm{x})\right)\right) d\mathrm{x} = f(\boldsymbol{\mu}). \tag{1.44}$$

Using identity (1.44) into our thermodynamic limit implies that

$$\lim_{N\to\infty} p_N(\boldsymbol{J},\boldsymbol{h}) = \lim_{N\to\infty}\left(\frac{1}{N}\ln(\sqrt{\frac{N\det\tilde{\mathbf{J}}}{(2\pi)^2}})\right) + \frac{1}{N}\ln(\int_{\mathbb{R}^2} \exp(N(f(\mathrm{x})))\, d\mathrm{x})$$

$$= \max_{\mathrm{x}} f(\mathrm{x})$$

Finally, the same consistency equations (1.42) is given by differentiating of the function $f$ (1.43) with respect to $x_1, x_2$.

## The Monomer-Dimer Model

Any way to fully match the vertices of a finite graph $G$ by non-overlapping dimers and monomers is called a monomer-dimer configuration. Based on such configuration, a monomer-dimer model with pure hard-core interaction can be defined by a probability corresponded to an exponential function of the number of dimers (or monomers). In particular these models were introduced to study the features of special molecules e.g. diatomic oxygen molecules and liquid mixtures with non-equal size of molecules. In the case of pure hard-core interactions, Heilmann and Lieb (1970 and 1972) proposed a rigorous proof of absence of phase transitions for both complete graph (the mean-field case) and the regular lattices. According to Heilmann and Lieb (1979), on certain 2-dimensional regular lattices, if there are attractive interactions among dimers with the same orientation, then there exists a phase transition at low temperatures. Very recently, there has been a considerable attention in the study of the mean-field case of the model (Alberici et al 2014). Namely, Alberici et al (2014) states that such mean-field model belongs to the mean-field ferromagnetic universality class. This section gives a brief discussion on the ferromagnetic mean filed Monomer-Dimer model with interaction among monomers and dimers: The Heilmann-Lieb approach for the pure hard-core interacting case is used in order to calculate upper and lower bounds for the pressure and then the consistency equation of the model is obtained.

## The Model

Consider a finite simple graph $G = (V, E)$ built over a vertex $V$ and edge set $E \subseteq \{uv \equiv \{u, v\} | u \neq v \in V\}$. We define a *dimer configuration* $D \subseteq E$ on the graph $G$ as a set of pairwise non-incident edges (*dimers*):

$$uv \in D \Rightarrow uw \notin D \; \forall w \neq v.$$

where the associated set of dimer-free vertices (*monomers*) is introduced by

$$\mathcal{M}(D) \coloneqq \mathcal{M}_G(D) \coloneqq \{u \in V | uv \notin D \; \forall v \in V\}.$$

Assume $\mathcal{D}_G$ is the set of all possible dimer configurations on the graph $G$. For a given dimer configuration $D \in \mathcal{D}_G$we set for all $v \in V$, $e \in E$:

$$\alpha_u(D) \coloneqq \begin{cases} 1, & \text{if } v \in \mathcal{M}(D) \\ 0, & \text{otherwise} \end{cases} \text{ and } \alpha_e(D) \coloneqq \begin{cases} 1, & \text{if } e \in E \\ 0, & \text{otherwise} \end{cases} \tag{1.45}$$

The Hamiltonian of *imitative monomer-dimer model* on the graph $G$ can be defined by assigning an imitation coefficient $J \geq 0$ and an external field $h \in \mathbb{R}$ as $H_G^{IMD}: \mathcal{D}_G \to \mathbb{R}$

$$H_G^{IMD} \coloneqq -\sum_{v \in V} h\alpha_v - \sum_{uv \in E} J(\alpha_u \alpha_v + (1 - \alpha_u)(1 - \alpha_v)). \tag{1.46}$$

The choice of the Hamiltonian allows us to express a Gibbs measure on the space of configurations $\mathcal{D}_G$ as:

$$\mu_G^{IMD} \coloneqq \frac{\exp(-H_G^{IMD}(D))}{Z_G^{IMD}} \;\; \forall D \in \mathcal{D}_G \tag{1.47}$$

where $Z_G^{IMD} = \sum_{D\in\mathcal{D}_G} \exp(-H_G^{IMD}(D))$ is the partition function of the model. The monomer density of the model is obtained by computing the derivative of the pressure per particle - $p_G^{IMD} = \ln( Z_G^{IMD})$ - with respect to $h$:

$$m_G^{IMD} = \sum_{D\in\mathcal{D}_G} \frac{|\mathcal{M}(D)|}{|V|} \mu_G^{IMD} = \frac{\partial}{\partial h}\frac{p_G^{IMD}}{|V|} \tag{1.48}$$

As $J = 0$, the model reduces to the one studied by Heilmann and Lieb (Heilmann and Lieb 1970; Heilmann and Lieb 1972). It is convenient to know that the reduced model is specified only by a topological interaction in which the hard-core constraint describes the space of states $\mathcal{D}_G$. Despite the fact that the topological interaction exists, Heilmann and Lieb (Heilmann and Lieb 1970; Heilmann and Lieb 1972) proved the absence of phase transition for such model. By setting the parameter $J \geq 0$, we can consider another type of interaction in the original model. That is, the state of a vertex has a significant influence on or determines the state of its neighbors pushing each other to behave in an analogous way. In this case, we need to consider a more general Hamiltonian than (1.46). Therefore, let us denote a monomer external field by $h^{(m)} \in \mathbb{R}$, a dimer eternal field by $h^{(d)} \in \mathbb{R}$, a monomer imitation coefficient by $J^{(m)} \in \mathbb{R}$, a dimer imitation coefficient by $J^{(d)} \in \mathbb{R}$ and a counter-imitation coefficient by $J^{(md)} \in \mathbb{R}$ and introduce the Hamiltonian:

$$\widetilde{H}_G^{IMD} \coloneqq - \sum_{v\in V} h^{(m)}\alpha_v - \sum_{e\in E} h^{(d)}\alpha_e - \sum_{uv\in E} J^{(m)}\alpha_u\alpha_v - \sum_{uv\in E} J^{(d)}(1-\alpha_u)(1-\alpha_v) - \sum_{uv\in E} J^{(md)}(\alpha_u(1-\alpha_v) + (1-\alpha_u)\alpha_v). \tag{1.49}$$

Using the valid relation $2|D| + |\mathcal{M}(D)| = |V|$ into the Hamiltonian (1.49) we have that:

$$\widetilde{H}_G^{IMD} \coloneqq -C' - \sum_{v\in V} h'\alpha_v - \sum_{uv\in E} J'\alpha_u\alpha_v - \sum_{uv\in E} J''(1-\alpha_u)(1-\alpha_v) \tag{1.50}$$

where $C' = \frac{|V|}{2}$ $h' = h^{(m)} - h^{(d)}/2$, $J' = J^{(m)} - J^{(md)}$, and $J'' = J^{(d)} - J^{(md)}$. Let us now rewrite the Hamiltonian (1.50) using the relation $\sum_{uv\in E}(\alpha_u + \alpha_v) = r|\mathcal{M}|$ when the graph $G$ is regular of degree $r$:

$$\widetilde{H}_G^{IMD} \coloneqq -C - \sum_{v\in V} h\alpha_v - \sum_{uv\in E} J(\alpha_u\alpha_v + (1-\alpha_u)(1-\alpha_v)) \tag{1.51}$$

where $h = h' + (J' - J'')r$, $J = (J' + J'')/2$ and $C = C' + (J'' - J')|E|$.

From the last identity it is observable that when the general Hamiltonian (1.50) defined on a regular graph then it is equivalent to the Hamiltonian (1.46). Moreover one can see here is that the imitation coefficient $J \geq 0$ corresponds to the $J^{(m)} + J^{(d)} \geq 2J^{(md)}$.

At this point, Let us to define our imitative monomer-dimer model on the complete graph $G = K_N = (V_N, E_N)$ with $V_N = \{1, \dots, N\}$ and $E_N = \{\{u,v\} | u, v \in V_N, u < v\}$. Accordingly, since the number of edges is of order $N^2$, we need to normalize the external field $h$ and the imitation coefficient $J$ for keeping the pressure of order $N$. Therefore, we can consider the Hamiltonian $H_N^{IMD}: \mathcal{D}_{K_N} \to \mathbb{R}$,

$$H_N^{IMD} \coloneqq -\sum_{v\in V_N} h\alpha_v + \ln(N)\sum_{e\in E_N}\alpha_e - \sum_{uv\in E_N}\frac{J}{N}(\alpha_u\alpha_v + (1-\alpha_u)(1-\alpha_v)), \tag{1.52}$$

where the partition function $Z_N^{IMD} = \sum_{D\in\mathcal{D}_{K_N}} \exp(-H_N^{IMD}(D))$ and the monomer density $m_N^{IMD} = \frac{\sum_{D\in\mathcal{D}_{K_N}} \frac{|\mathcal{M}(D)|}{N} \exp(-H_N^{IMD}(D))}{Z_N^{IMD}}$.

## The Thermodynamic Limit

It is easy to verify that the relation $2|\mathcal{D}_{K_N}| + |\mathcal{M}_{K_N}| = |V_N|$ is hold and since the graph $K_N$ is regular of degree $N-1$ we have that:

$$\sum_{uv\in E_N}(\alpha_u + \alpha_v) = (N-1)|\mathcal{M}_{K_N}|.$$

These identities help us to express the Hamiltonian (1.46) in the form:

$$H_N^{IMD} = \frac{N}{2}\ln(N) - \frac{(N-1)}{2}J - \left(h + \frac{1}{2}\ln(N) - J\right)\sum_{v\in V_N}\alpha_v - \frac{J}{N}\left(\sum_{v\in V_N}\alpha_v\right)^2$$

The identity $\sum_{v\in V_N}\alpha_v = Nm_N$ where $m_N(D) = \frac{|\mathcal{M}_{K_N}(D)|}{N} \in [0,1]$ allow us to rewrite the Hamiltonian in the mean-field form as:

$$H_N^{IMD} = -N(Jm_N^2 + b_N m_N + c_N) \qquad (1.53)$$

where $b_N = \frac{1}{2}\ln(N) + h - J$, $c_N = -\frac{1}{2}\ln(N) + \frac{N-1}{2N}J$, and consequently, the partition function of the system $Z_N^{IMD}$ leads to consider the pressure function per particle:

$$p^{IMD} = \lim_{N\to\infty}\frac{\ln(Z_N^{IMD})}{N} \qquad (1.54)$$

To show the existence of the thermodynamic limit of the pressure for the imitative monomer-dimer model as $N \to \infty$, let us consider the Hamiltonian without imitation $H_N^{MD}: \mathcal{D}_G \to \mathbb{R}$:

$$H_N^{MD} \coloneqq -\sum_{v\in V_N} h\alpha_v + \ln(N)\sum_{e\in E_N}\alpha_e, \qquad (1.55)$$

with the partition function $Z_N^{MD} \coloneqq \sum_{D\in\mathcal{D}_{K_N}}\exp(-H_N^{MD}(D))$ and the monomer density $m_N^{MD} = \frac{\sum_{D\in\mathcal{D}_{K_N}}\frac{|\mathcal{M}(D)|}{N}\exp(-H_N^{MD}(D))}{Z_N^{MD}}$. Proposition 6 proved by Alberici et al (2014) stats that for $h \in \mathbb{R}$, the pressure per particle of the monomer-dimer model on the complete graph defined by Hamiltonian (1.55) admits finite thermodynamic limit:

$$\lim_{N\to\infty}\frac{\ln(Z_N^{MD})}{N} = p^{MD}(h) \qquad (1.56)$$

where $\forall x \in \mathbb{R}$:

$$p^{MD}(x) = -\frac{1-g(x)}{2} - \ln\big(g(x)\big) + x, \qquad (1.57)$$

with

$$g(x) = \frac{1}{2}(\sqrt{e^{4x} + 4e^{2x}} + e^{2x}). \qquad (1.58)$$

Using the Proposition 6 proved by Alberici et al (2014) and the Hamiltonian (1.53) allow us to propose the following theorem for showing the existence of the thermodynamic limit:

**Theorem 1.3.** Let $h \in \mathbb{R}$ and $J \geq 0$. The pressure per particle of the imitative monomer-dimer model on the complete graph defined by Hamiltonian (1.52) admits finite thermodynamic limit:

$$\lim_{N\to\infty} \frac{\ln(Z_N^{IMD})}{N} = p^{IMD} = \sup_m \tilde{p}(m) \tag{1.59}$$

with

$$\tilde{p}(m) = -Jm^2 + \frac{1}{2}J + p^{MD}\big((2m-1)J + h\big) \quad \forall m \in \mathbb{R} \tag{1.60}$$

where $p^{MD}()$ is defined by (1.57).

***Proof.*** To prove the theorem we need to compute the lower and upper bounds of the pressure per particle as follow:

[**Lower Bound**] Assume $m \in \mathbb{R}$ and $m_N(D) = \frac{|\mathcal{M}_{K_N}(D)|}{N} \in [0,1]$ then $(m_N(D) - m)^2 \geq 0$ follows that

$$m_N(D)^2 \geq 2mm_N(D) - m^2.$$

Using the last inequality with assumption $J \geq 0$ into the mean-field Hamiltonian (1.53) we observe that

$$-H_N^{IMD}(D) = N(Jm_N(D)^2 + b_N m_N(D) + c_N) \geq N((2Jm + b_N)m_N(D) - Jm^2 + c_N)$$

and for partition function as well:

$$Z_N^{IMD} = \sum_D \exp(-H_N^{IMD}) \geq \sum_D \exp(N((2Jm + b_N)m_N(D) - Jm^2 + c_N)) =$$

$$= e^{Ny_N(m)} Z_N^{MD}(x(m))$$

where $y_N(m) = -Jm^2 + \frac{N-1}{2N}J$ and $x(m) = 2Jm + h - J$.

[**Upper Bound**] $m_N$ takes $N+1$ values which can be shown as the elements of the set $\Sigma_N = \{0, \frac{1}{N}, \dots, 1 - \frac{1}{N}, 1\}$. The definition of the Kronecker delta $\delta_{m,m_N(D)}$ for every $m_N(D)$ in the form of $\sum_{m_N(D)\in\Sigma_N} \delta_{m,m_N(D)} = 1$, writing $F(m_N(D)^2)\delta_{m,m_N(D)} = F(2mm_N(D) - m^2)\delta_{m,m_N(D)}$ for any function $F$, and by using the mean-field Hamiltonian (1.53) we can say

$$\delta_{m,m_N(D)} \exp\big(-H_N^{IMD}(D)\big) = \delta_{m,m_N(D)} \exp(N(Jm_N(D)^2 + b_N m_N(D) + c_N)) =$$

$$= \delta_{m,m_N(D)} \exp(N((2Jm + b_N)m_N(D) - Jm^2 + c_N))$$

and as a consequence we can obtain

$$Z_N^{IMD} = \sum_D \sum_{m_N(D)\in\Sigma_N} \delta_{m,m_N(D)} \exp\big(-H_N^{IMD}(D)\big) =$$

$$= \sum_D \sum_{m_N(D)\in\Sigma_N} \delta_{m,m_N(D)} \exp(N((2Jm + b_N)m_N(D) - Jm^2 + c_N)) \leq$$

$$\leq \sum_m \sum_D \exp\Big(N\big((2Jm + b_N)m_N(D) - Jm^2 + c_N\big)\Big) =$$

$$= \sum_m e^{Ny_N(m)} Z_N^{MD}(x(m)) \leq (N+1) \sup_{m\in[0,1]} \{e^{Ny_N(m)} Z_N^{MD}(x(m)\}$$

Now we can put together the bounds and found that

$$\sup_{m\in[0,1]} \{e^{Ny_N(m)} Z_N^{MD}(x(m)\} \leq Z_N^{IMD} \leq (N+1) \sup_{m\in[0,1]} \{e^{Ny_N(m)} Z_N^{MD}(x(m)\}$$

We then proceed by taking the logarithm and dividing by $N$:

$$\frac{\ln\left(\sup_{m\in[0,1]} \{e^{Ny_N(m)} Z_N^{MD}(x(m)\}\right)}{N} \leq \frac{\ln(Z_N^{IMD})}{N} \leq \frac{\ln\left((N+1) \sup_{m\in[0,1]} \{e^{Ny_N(m)} Z_N^{MD}(x(m)\}\right)}{N}$$

$$0 \leq \frac{\ln(Z_N^{IMD})}{N} - \sup_{m\in[0,1]} \{y_N(m) + \frac{\ln(Z_N^{MD}(x(m)))}{N}\} \leq \frac{\ln(N+1)}{N} \xrightarrow[N\to\infty]{} 0$$

Since the pressure per particle $h \mapsto \frac{\ln(Z_N^{MD}(h))}{N}$ is a convex function, as $N \to \infty$ the convergence $\frac{\ln(Z_N^{MD}(h))}{N} \mapsto p^{MD}(h)$ is uniform in $h$ on compact sets. On the other hand, $y_N(m)$ uniformly converges to $y(m) \coloneqq -Jm^2 + \frac{1}{2}J$ in $m$ when $N \to \infty$. Thus, one has that $y_N(m) + \frac{\ln(Z_N^{MD}(x(m)))}{N}$ converges uniformly to $y(m) + p^{MD}(x(m))$ in $m$ as $N \to \infty$ on compact sets. As a result we have

$$\sup_{m\in[0,1]} \{y_N(m) + \frac{\ln(Z_N^{MD}(x(m)))}{N}\} \xrightarrow[N\to\infty]{} \sup_{m\in[0,1]} \{y(m) + p^{MD}(x(m))\}$$

and it concludes the proof: $p^{IMD} = \lim_{N\to\infty} \frac{\ln\left(Z_N^{IMD}\right)}{N} = \sup_{m\in[0,1]}\{\tilde{p}(m)\}$ where $\tilde{p}(m) = y(m) + p^{MD}(x(m))$. ■

### The Solution

Let us now consider the derivative of the function $\tilde{p}$:

$$\frac{\partial \tilde{p}(m)}{\partial m} = \frac{\partial y(m)}{\partial m} + \frac{\partial p^{MD}(x(m))}{\partial m}.$$

Using proposition 6 proved by Alberici et al (2014), we have that $(p^{MD})' = g$ and as well:

$$\frac{\partial \tilde{p}(m)}{\partial m} = \frac{\partial\left(-Jm^2 + \frac{1}{2}J\right)}{\partial m} + \frac{\partial x(m)}{\partial m} g(x(m)).$$

Therefore,

$$\frac{\partial \tilde{p}(m)}{\partial m} = -2Jm + 2Jg((2m-1)J + h). \tag{1.61}$$

If we compute $\frac{\partial \tilde{p}(m)}{\partial m} = 0$ then we have the self-consistency equation of the model:

$$m = g((2m-1)J + h) \tag{1.62}$$

One observe that the function $m \mapsto \tilde{p}(m)$ attains its global maximum inside the interval $[0,1]$ since for all $m \leq 0$ $\frac{\partial \tilde{p}(m)}{\partial m} > 0$ and for all $\geq 1$ $\frac{\partial \tilde{p}(m)}{\partial m} < 0$. Moreover, any global maximum point $m^*$ of $\tilde{p}$ is a critical point satisfies the equation (1.62). As mentioned earlier, since $\frac{1}{N}\ln(Z_N^{IMD}(h,j))$ is a convex function of $h$, as $N \to \infty$ it converges to $p^{IMD}(h,J) = \tilde{p}(m^*(h,J),h,J)$. If $m^*(h,J)$ be differentiable in $h$ then we get:

$$\frac{\partial p^{IMD}}{\partial h} = \frac{\mathrm{d}}{\mathrm{d}h}\tilde{p}(m^*(h,J),h,J) = \underbrace{\frac{\partial \tilde{p}(m^*)}{\partial m}}_{=0}\frac{\partial m^*}{\partial m} + \underbrace{\frac{\partial \tilde{p}}{\partial h}}_{=(p^{MD})'=g} = g\big((2m^*-1)J + h\big) = m^*.$$

# STUDY OF THE PHASE TRANSITION SINGULAR SURFACE

The theory of phase transition considers the transformation of a thermodynamic system from one phase or state to another. Such transformation occurs when there is a singularity in the free energy or one of its derivatives (Yeomans 1992). As presented in previous chapter, the mean-field theory gives us a simple and efficient tool to describe the ferromagnetic systems. A main goal of these attempts is to achieve an accurate description of magnetic and ferromagnetic materials that can predict the detailed atomic structure and associated phase transitions as a function of, for example, temperature, external field and etc (Yeomans 1992; Kochmanski et al 2013). Clearly, only with such knowledge one can understand the physical properties of these materials. In this way, for example, the solution of self-consistency equation associated with the system often helps us to study the phase transition phenomena with more details namely the location of the jump. Since, those equations are in the form of transcendental equations; we cannot solve them algebraically. Therefore, shaping the phase transition can be done numerically by relying on two ways: numerical maximization of the pressure function or numerical solution of the self-consistency equation. The first one could be performed by using an appropriate optimization technique to find the global maximums of the pressure[1]. On the other hand, the second one can be done by using a suitable numerical root-finding method to obtain the zeroes of implicit form of those equations. In this part of the study, depending on the type of each implicit form, we suggest an appropriate root-finding algorithm for finding these zeros in order to draw the shape of phase transition surface: the *Brent-*

---

[1] One of the best choices here is using *Cutting Angle Method* (CAM). CAM is a global search introduced based on the results in abstract convexity (Christodoulos, and Panos 2008). It was first proposed by Andramonov et. al. (1999) and extended by Rubinov (2000) for optimization of the increasing convex- along-rays functions and also developed by Seyedi (2010) to apply for minimization of variational problems (and in particular optimal control problems). As a special case, the CAM is a generalization of the Cutting Plane Method from convex minimization. It can be applied in a very broad class of non-convex global optimization problems in which the functions involved possess suitable generalized affine minorants (Rubinov 2000; Christodoulos and Panos 2008).

*Dekker* method (Dekker 1969; Brent 1973) for one population cases (*Curie-Weiss case* and *monomer-dimer system*), and the *trust-region* algorithm (Conn et al 2000) for *bipartite Curie-Weiss model*. We then summarize the result of numerical solutions in the phase transition diagram for each model to show the exact location of the jump.

## The Curie-Weiss Model

Let us look at the *Curie-Weiss* model defined by mean field Hamiltonian (1.4) where its self-consistency equation (1.22) obtained in the previous chapter. Since this equation cannot solve algebraically, we need to rely on a numerical approach which are designed either for numerical maximization of $p_{lower}(\widetilde{m})$ (or $p_{upper}(\widetilde{m})$) or for numerical solution of mean-field equation (1.22). Indeed, the solutions of self-consistency equation (1.22) are the points of intersection between the curve $y_1(\widetilde{m}) = tanh(J\widetilde{m} + h)$ and the line $y_2(\widetilde{m}) = \widetilde{m}$. One can observe here is that for any positive value of $J$, if $h \neq 0$, we have only one intersection point between these two functions which is nonzero (see the lower panels of figures 2.1). That is, as can be seen in the lower panel of the figure 2.2, when the equation (1.22) admits only one solution then the solution is a unique maximum for $p_{lower}(\widetilde{m})$. On the other hand, for $h = 0$ we have two different cases: As can be seen in the upper left panel of the figure 2.1, if $J \leq 1$ then there is only one intersection point, the zero which is the unique maximum of the function $p_{lower}$ (see the upper left panels of figure 2.2). But when $J > 1$ we have two intersection points $\pm\widetilde{m}_0$, namely there are 2 maximums for $p_{lower}$ (see the upper right panels of figures 2.1 and 2.2).

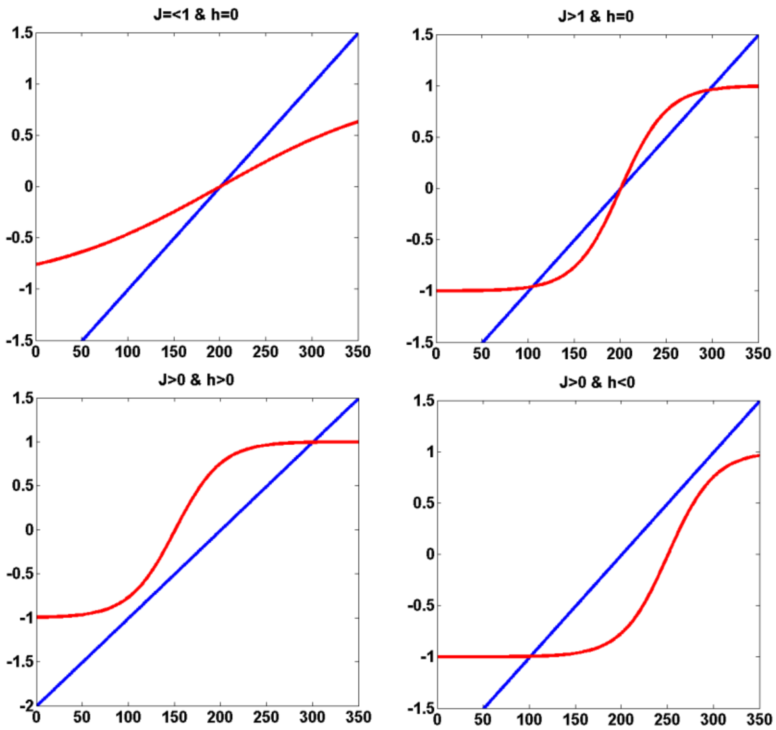


**Figure 2.1.** The number of points of intersection between the red curve $y_1(\tilde{m}) = tanh(J\tilde{m} + h)$ and the blue line $y_2(\tilde{m}) = \tilde{m}$.

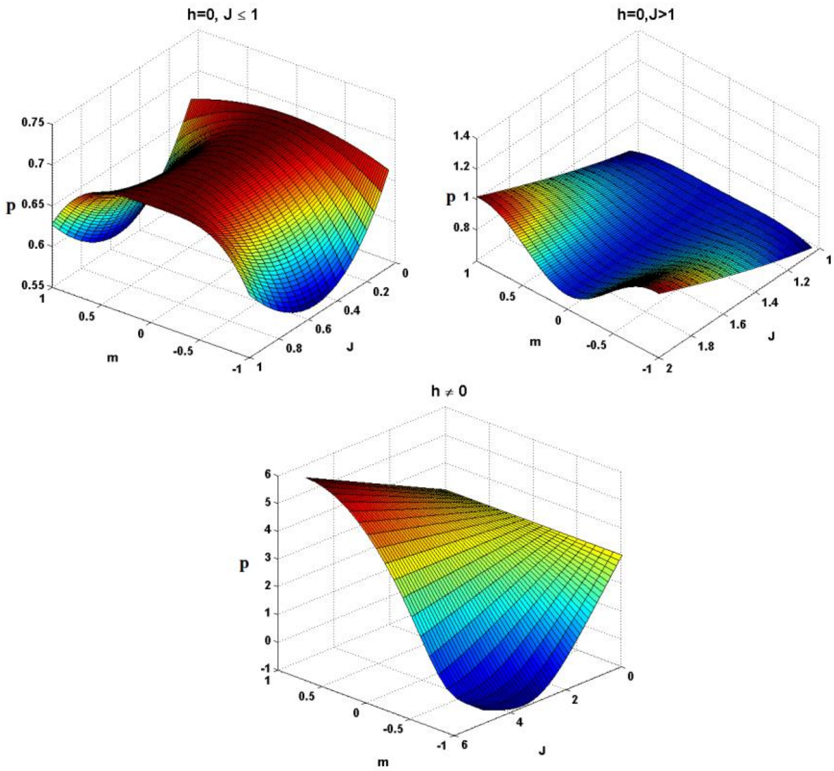


**Figure 2.2.** *The Curie-Weiss Critical points*: The pressure function admits one peak except when the external field vanishes and the coupling constant becomes greater than its critical value $J_c = 1$.

This detailed graphical approach can be simply converted into the problem of numerically finding the roots of the implicit function

$$\tilde{m} - tanh(J\tilde{m} + h) = 0. \tag{2.1}$$

Finding the roots of this implicit equation could be numerically achieved by using the iteration method suggested by T. Dekker (Dekker 1969). The method is a kind of complicated root-finding algorithm that combines the bisection, secant, and inverse quadratic interpolation methods. Therefore, by taking $h$ and $J$ the groups of values for different values of solution $\tilde{m}$, the plot of $(J, h)$ versus $\tilde{m}$ gives typical information about the mechanism of phase transition and in particular the location of the jump. We summarized the result of this detailed procedure in the figure 2.3.

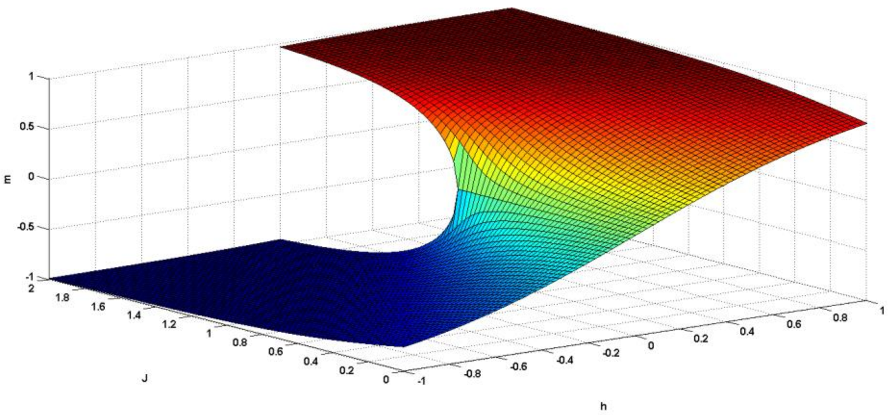


**Figure 2.3.** $\langle m \rangle$ as function of $J$ and $h$ for one population *Curie-Weiss* case.

Figure 2.3 shows that when $h$ is different from zero there is no phase transition, but in the absence of field $h$ we have totally different situation:

$$\lim_{N\to\infty} p_N(J,0) = \begin{cases} 0 & J \leq 1 \\ \ln(2) - \frac{J}{2}\tilde{m}_0^2 + \ln(\cosh(J\tilde{m}_0)) & J > 1 \end{cases}$$

That is, the spontaneous magnetization $\tilde{m}_0$ tends to zero as $J \to 1^+$. Thus, it follows that $\forall J$ the limit of the pressure is continuous and we have that:

$$\frac{\partial}{\partial J}\left(\lim_{N\to\infty} p_N(J,0)\right) = \begin{cases} 0 & J \leq 1 \\ \frac{1}{2}\tilde{m}_0^2 & J > 1 \end{cases}$$

and in the same way for the second derivative we can obtain:

$$\frac{\partial^2}{\partial J^2}(\lim_{N\to\infty} p_N(J,0)) = \begin{cases} 0 & J \leq 1 \\ \frac{1}{2}\frac{d\tilde{m}_0^2}{dJ} & J > 1 \end{cases} \tag{2.2}$$

Since the value of $\tilde{m}_0$ is very small when the value of $J$ is very close to 1 from the left, the hyperbolic tangent of the equation (1.22) can be expanded by

$$\tilde{m}_0 = J\tilde{m}_0 - \frac{(J\tilde{m}_0)^3}{3} + O(\tilde{m}_0^5) \qquad \text{as } J \to 1^+ \tag{2.3}$$

Now we can divide the equation (2.3) by $J\tilde{m}_0$ because $\tilde{m}_0$ is nonzero and so we have:

$$\frac{1}{J} = 1 - \frac{(J\tilde{m}_0)^2}{3} + O(\tilde{m}_0^4) \qquad \text{as } J \to 1^+$$

It implies that as $J \to 1^+$: $\tilde{m}_0 \sim \left(3\left(1-\frac{1}{J}\right)\right)^{\frac{1}{2}}$ and consequently we can approximate the value of $\frac{1}{2}\frac{d\tilde{m}_0^2}{dJ}$ inside the identity (2.2) as:

$$\frac{1}{2}\frac{d\tilde{m}_0^2}{dJ} \sim \frac{3}{2J^2} \qquad \text{as } J \to \frac{1^+}{J}$$

Hence, the second derivative of the thermodynamic limit of the system is not continuous. Thus, as can be seen in figure 2.3, the *Curie-Weiss* model exhibits a phase transition of the second order for $h = 0$ and $J = 1$.

## The Bipartite Curie-Weiss Model

This part is dedicated to numerical study of phase transition occurs in bipartite mean field *Curie-Weiss* model. To do so, consider our bipartite model defined by its Hamiltonian (1.27) and the bipartite mean field equation (1.42). In this section we use different numerical method, so-called *trust-region* algorithm (Conn et al 2000) due to the fact that the equation (1.42) is a system of transcendental equations.

To start our numerical study, we first invert the system (1.42) into the following form because $J_{12} \neq 0$:

$$\begin{cases} m_2 = \frac{1}{(1-\alpha)J_{12}}(\tanh^{-1}(m_1) - \alpha J_{11} m_1) \\ m_1 = \frac{1}{\alpha J_{12}}(\tanh^{-1}(m_2) - (1-\alpha)J_{22} m_2) \end{cases} \tag{2.4}$$

This reformulation lends itself to a graphic resolution. Therefore, let us consider the Cartesian coordinate system $m_1 m_2$ and also define the following functions:

$$\begin{gathered} y_1(m_1) = \frac{1}{(1-\alpha)J_{12}}(\tanh^{-1}(m_1) - \alpha J_{11} m_1) \\ y_2(m_1) = \frac{1}{\alpha J_{12}}(\tanh^{-1}(m_1) - (1-\alpha)J_{22} m_1) \end{gathered} \tag{2.5}$$

We then proceed by denoting $f_1$ and $f_2$ as the graph of two functions $y_1$ and $y_2$ respectively. One has that the intersections between $f_1$ and $\hat{f}_2$ with respect to the line $m_2 = m_1$ are the solutions of the system (2.4) where $\hat{f}_2$ is the symmetrical curve of $f_2$. For more understanding, for instance, the classic visual representation of this numerical approach is presented in figure 2.4 when there is only one solution.

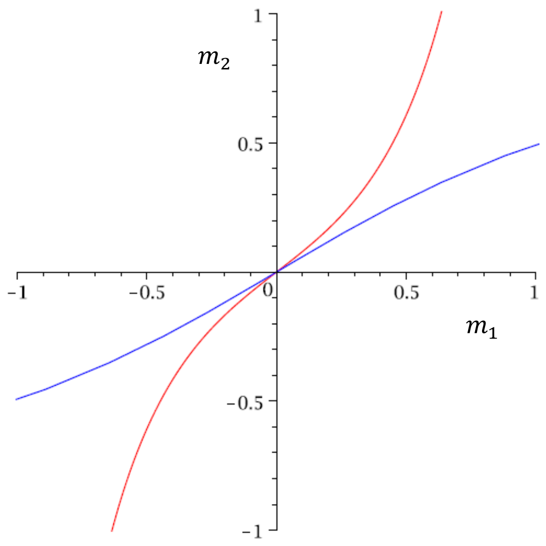


**Figure 2.4.** Graphic representation of the system (2.4) when there is a unique solution. The red and blue curves indicate $f_1$ and $\hat{f}_2$ respectively when we assumed $J_{12} > 0$.

This graphical approach can be easily converted into numerically finding the roots of implicit form of the system (1.42). Obtaining these roots can be numerically achieved by using *trust-region* algorithm (Conn et al 2000). The results of this application are summarized in the figure 2.5. It is convenient to say that the system (1.42) has generally nine solutions and four of which are stable solutions corresponding to relative maxima of the pressure (for more details see (Gallo and Contucci 2008)).

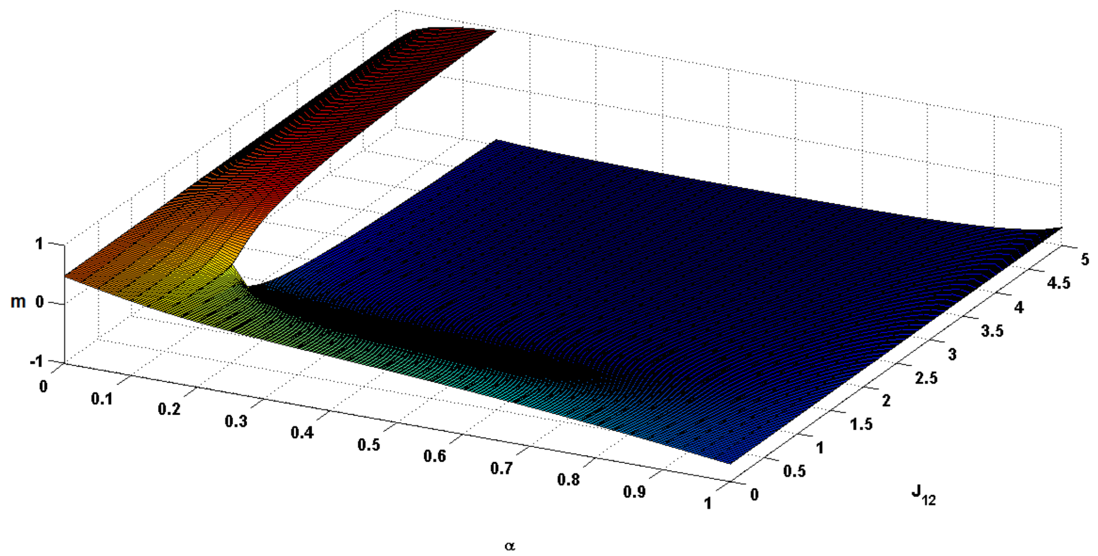


**Figure 2.5.** $\langle m \rangle$ as a function of $\alpha$ and $J_{12}$. In this numerical study we fixed $J_{11} = 0.9, J_{22} = 1.01, h_1 = -0.2373$ and $h_2 = 0.0443$.

Figure 2.5 displays the total average magnetization $\langle m \rangle$, which is the main quantity we study here, as a function of $\alpha$ and mutual interaction $J_{12}$. What we see here in our findings is, when the mutual interaction $J_{12}$ is small enough, the magnetization $m$ is smoothly varying in $\alpha$ from $m_2$ to $m_1$. But, as can be seen in the figure 2.5, when the interaction parameter $J_{12}$ crosses its critical value $J_{12}^c = 1.15$ (where $\alpha^c = 0.05$ and $m^c = 0.9165$), the magnetization exhibits a discontinuous transition in the absence of external magnetic field. One has that the value of $\alpha^c$ depends on parameters $J_{11}$, $J_{22}$, $m_1$, and $m_2$. This means that this critical value does not depends on parameter $J_{12}$.

## The Monomer-Dimer Model

To complete the numerical study part, reconsider the mean-filed monomer-dimer model defined by its Hamiltonian (1.53). In this model, to identify the stationary points of function $\tilde{p}(m,J,h)$ defined by (1.60) we first need to compute the first and second derivative of this function with respect to $m$ as follow:

$$\frac{\partial \tilde{p}}{\partial m}(m,J,h) = -2Jm + 2Jg((2m-1)J + h) \tag{2.6}$$

$$\frac{\partial^2 \tilde{p}}{\partial m^2}(m,J,h) = -2J + (2J)^2 g'((2m-1)J + h) \tag{2.7}$$

where the function $g$ is defined by (1.58) and remember that $(p^{MD})' = g$. Since the value of $g$ ranges in the interval (0,1), it implies to say that $\forall J > 0$ and $h \in \mathbb{R}$ there are:

$$\frac{\partial \tilde{p}}{\partial m}(m,J,h) > 0 \ \forall m \in (-\infty, 0] \text{ and } \frac{\partial \tilde{p}}{\partial m}(m,J,h) < 0 \ \forall m \in [1, \infty) \tag{2.8}$$

Thus, one observable here is that the function $\tilde{p}(m,J,h)$ admits at least one maximum $m = m^*(J,h) \in (0,1)$ which satisfies the following conditions:

$$\frac{\partial \tilde{p}}{\partial m}(m,J,h) = 0 \quad \text{i.e.} \quad m = g((2m-1)J + h) \tag{2.9}$$

$$\frac{\partial^2 \tilde{p}}{\partial m^2}(m,J,h) \le 0 \quad \text{i.e.} \quad g'((2m-1)J + h) \le \frac{1}{2J} \tag{2.10}$$

The stationary points characterized by equation (2.9) cannot be solved algebraically. Therefore, we need to suggest a numerical approach to solve such transcendental equation. However, the properties and approximation of these values also can be identified and determined by studying the inequality (2.10). Let us now perform the same operations which were done for one population *Curie-Weiss* case. For doing this, consider the equation (2.9). We convert the graphical representation of numerical finding the intersections between the line $y_1 = m$ and the curve $y_2 = g((2m-1)J + h)$ into numerically finding the roots of implicit form of equation (1.62):

$$m - g((2m-1)J + h)=0 \qquad (2.11)$$

Similar to Alberici et al (2014)'s findings, we observe that for rising $J$ from 0 to its critical value $J_c$, the line $y_1$ and the curve $y_2$ has a unique intersection while the interacting coupling becomes greater that its critical value we have three different situations:

- If $\psi_1(J) \leq h \leq \psi_2(J)$, then there exist three intersections
- If $h = \psi_1(J)$ or $h = \psi_2(J)$, then there are two intersections
- And if $h \leq \psi_1(J)$ or $h \geq \psi_2(J)$, then there is only one intersection

where

$$\psi_i(J) = J + \frac{1}{2}\log\big(a_i(J)\big) - 2Jg(\frac{1}{2}\log\big(a_i(J)\big)) \text{ for } i = 1,2$$

with

$$a_i(J) = \frac{-\left(\frac{1}{(2J)^2}+\frac{8}{2J}-4\right)+(-1^{i})\left(2-\frac{1}{2J}\right)\sqrt{\frac{1}{(2J)^2}-\frac{12}{2J}+4}}{\frac{4}{2J}}.$$

We now proceed by using the *Brent-Dekker* method similar to one population *Curie-Weiss* case. In terms of numerical root finding, one has that there are multiple roots for equation (2.11) that we need to compute and evaluate, corresponding to the stability of the solutions. The methodology for obtaining the various roots $m_0$ is numerically intensive. Hence, we divide the interval of magnetization-values into multiple sub-intervals in order to search for finding the multiple roots. In terms of programming, this becomes a complicated problem. But this can be controlled by a precise description of initial points which are used for our iteration method (the *Brent-Dekker* method) in each subinterval. The results of this detailed work are summarized in the figure 2.6.

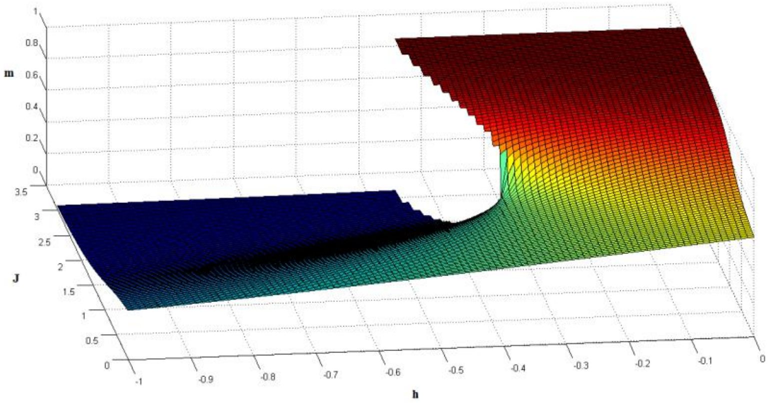


**Figure 2.6.** $\langle m \rangle$ as function of $J$ and $h$ for *Monomer-Dimer* Model with attractive interactions.

Figure 2.6 explains that the model exhibit a phase transition starting from $J_c = 1.47$ (where $m_c = 0.4655$, $h_c = -0.35$) toward asymptote $h = -0.5$. A main observable feature of this model, as can be seen in the figure 2.6, is that there exists an asymptotic wall when the phase transition occurs. These findings are agreed with the results of relevant research performed by Alberici et al (2014).

# AN APPLICATION TO SOCIO-ECONOMICS PROBLEMS

The research reported here addresses the problem of forecasting immigrant integration. The question we are concerned with is; if immigration rise by say 2 to 3 % would this affect the level of immigrant integration in the social system under study? If so, what is the effect magnitude? And finally, how precisely can we forecast it? To this end we develop and introduce a theoretical and mathematical forecasting framework. We expose the resulting model to exceptionally rich integration data from Spain. The empirical tests show that our model deliver precise forecasts of future immigrant integration levels, in multiple integration contexts, and for the entire timespan for which data is available.

Uncovering ways to forecast integration is a potentially important task. The integration of immigrants is and has long been a political priority in countries receiving immigration (European Commission 2005; Penninx et al. 2008; Jacoby et al. 2013). For example, achieving a minimum of integration is considered a necessity, to avoid friction and conflict between immigrants and natives in the host society (Castles and Miller 2009; Niessen and Huddleston 2010; European Commission 2011; IOM 2011; European Commission 2014). Furthermore, and perhaps most importantly, as the effects of low birth rates and aging populations are becoming manifest, high levels of immigrant integration or assimilation is considered by some of the world's leading economies key in building a competitive and sustainable economy for the future (European Commission 2010; European Council 2010; Giovagnoli 2011; Canada Government 2012).

However, the capacity to formulate effective integration policies hinges on the availability of scientific theories and works generating strong predictions of how the integration phenomenon is likely to unfold with the passing of time, and in the face of changing levels of immigration. While there is a rich demographic, sociological and economic literature on individual integration outcomes (see, for example, Van Tubergen (2006) for a good overview of this literature), the problem of forecasting the level of integrations in a society is largely ignored by past and contemporary research. Hence, by filling an important gap in the literature on immigrant integration, the research reported here constitutes a significant contribution to our knowledge about integration and integration phenomena.

The chapter is organized as follows. First we introduce the integration concept we aim at forecasting. Thereafter we introduce the theoretical and mathematical model of the integration phenomena on which we base our forecasting method, followed by data description. Then we present the methodological procedure, produce the forecasts, and conduct the proper evaluation of these forecasts. Finally, we conclude with a brief discussion of the wider implications of our results.

## Immigrant Integration

What is immigrant integration and what is it that we set out to forecast? Instead of engaging in the complex task of defining and operationalizing integration, we feel comfortable to adopt a pragmatic approach. For example, there is a consensus within and across demographic, sociological and economic disciplines that inter–marriage/inter–partnerships and immigrant labor force participation are core measures of social and socio–economic immigrant integration (see Gordon 1964; Alba and Nee 1997; Raijman and Tienda 1999; Van Tubergen 2006 for a more extensive discussions on the relevance of these integration quantifiers). Therefore, in the research reported here we set out to develop a quantitative forecasting model capable of predicting integration in the form of inter–partnerships and immigrants labor market participation. More specifically, we have suitable data available for the following four integration quantifiers; 1) rate of inter–marriage between native and foreign born, 2) rate of newborns with one native and one foreign parent, 3) rate of indefinite labor contracts given to immigrants, and 4) rate of temporary labor contracts given to immigrants (see further in the section Data Description below). The former are example of social integration quantifiers, while the latter are examples of so called socio–economic integration quantifiers.

## A Simple Model of a Complex Phenomenon

Forecasting integration requires a reliable and efficient model of the integration phenomena. Past research has shown that both individual and contextual factors are important when explaining variation in immigrant integration outcomes (Van Tubergen and Maas 2007). For example, systematic differences in individual integration outcomes are often associated with age, sex, education, language proficiency, and other individual characteristics (Stevens and Swicegood 1987; Hwang et al. 1997; Cortina et al. 2008; Qian et al. 2012). Likewise, contextual factors, such as culture, ethnic–group–size, and local heterogeneity levels are influential when assessing inter–marriage propensities and labor market participation across different groups (Blau et al. 1982; Blau et al. 1984; Portes and Zhou 1993; Qian et al. 2012).

However, here our aim is not to forecast individual integration outcomes. Rather, we are interested in forecasting the trend in integration. That is, we are foremost concerned with the systemic evolution of integration quantifiers, in the presence of “noise” such as factors unique to individuals and their context.

Forecasting the trend in integration calls for a different type of model than what we typically see in contemporary research articles on integration and assimilation. In recent years, there have been considerable efforts to apply ideas and techniques from statistical physics to other areas of science such as economic, finance, social science, and biology. Explaining the social phase transition, modeling collective animal behavior, like natural flocks of birds, and predicting trends and crisis in the financial markets are some well–known examples of this venture (see Mantegna and Stanley

1999; Castellano et al. 2000; Bouchaud and Potters 2004; Levy 2005; Ballerini et al. 2008; Contucci et al. 2008; Stanley 2008; Bialek et al. 2012). This genre of models has recently been used to study also migration and integration phenomenon (Contucci and Giardina 2008; Barra and Contucci 2010; Barra et al. 2014).

Barra et al. (2014) have produced a theoretical framework of an immigrant–native system in which they successfully model the systemic integration process for social and socio–economic integration quantifiers as a function of immigrant density ($\gamma$).[2] In this work, and using integration data from Spain, they showed that a complicating, but yet intriguing, factor when modeling integration as a function of $\gamma$, is that while labor participation rates grow proportionally to immigrant density, the rates of inter–partnership have a growth law proportional to the square root of the immigrant density.

The different growth processes have well accepted individual solutions. For example, in a two–group system such as a society composed of immigrants and natives, there can be in–group or cross–group couplings. In other words the choice between, say, marrying or hiring an immigrant over a native is dichotomous. A natural candidate to describe the frequency of cross–group couplings in large populations is McFadden's Discrete Choice theory (McFadden 2001). A crucial assumption in the discrete choice theory is mutual independence between the involved random variables (Gallo et al. 2009). Consequently, McFadden's theory would predict linear growth in integration over immigrant density— $\gamma$. And indeed, McFadden's theory works very well when assessing the level of labor market integration as a function of immigration density (Barra et al. 2014). Hence, based on this finding it can be argued that the decisions of contracting an immigrant

---

[2] It should be noted that the causal relationship between immigrant group size and integration has received ample attention in Blau et al. 1982 and Blau et al. 1984. Blau et al’s findings are not contradictory to Barra et al. (2014) work, but complementary. However, in difference with Blau et al, Barra et al model the interaction component explicitly.

are made in a mutually independent fashion, regardless of how other actors have decided in this matter[3].

However, the square root growth in the rate of inter–partnerships suggests that the choice of partner is not well described by the classical discrete choice theory. A plausible source for this mismatch is that in difference to decisions in the labor market, inter–partnership decisions are not taken independently (Weber 1978; Barra et al. 2014). That is, the action of marrying an immigrant or having a child with an immigrant is a decision that is contingent of how others in the environment have acted or not acted in this context before the decision at hand (see also, for example, Kalmijn's (1998) discussion of social determinants in inter–marriage). Theories that relax the assumption of independence and cater to this type of social action and interaction, introduced by Brock and Durlauf (2001) and thereafter further developed (Contucci et al. 2008; Contucci and Giardina 2008; Gallo et al. 2009), predict a square root behavior of the probability of cross–group couplings. This finding is consistent with the growth law observed for the inter–partnership data by Barra et al (2014). That is, data suggest that social network activity induces the intensity of inter–partnerships.

The novelty introduced by Barra et al. (2014), is a mathematical framework that makes it possible to model the two different growth processes in a unified manner. The proposed solution is a generalization of the *monomer–dimer* model with the addition of an imitative interacting social network component with random topology in agreement with the small world–scenario (Watts and Strogatz 1998). The resulting model reduces to the classical discrete choice theory with linear growth in situations when social action and interaction in the integration process is negligible, and

[3] Note that the absence of interaction in labor market participation couplings does not mean that social networks are irrelevant in the job market. What the data analysis suggests is simply that the propensity of hiring immigrants over natives is unaffected by whether other employers have or have not hired immigrants over natives before. Social networks are still likely to be determinant for the individuals' chances of landing a job (see Granovetter 1974 on the latter).

to the square root behavior when such factors are prevailing (Barra et al, 2014). When confronted with empirical data the model provides an extraordinary fit across all integration quantifiers regardless of the a priori differences in the importance of social action and interaction discussed above[4].

Consequently, it can be shown that the level of integration in a society can be modeled mathematically as a function of immigrant density— $\gamma$ (Barra et al. 2014). Moreover, if the goal is to obtain estimates of the development of the general level of integration in a society as a function of $\gamma$ the model proposed by Barra et al. (2014) does a better job than the currently available alternatives. In what follows we will draw on this work as we develop a theoretical and quantitative framework to forecast integration as a function of immigrant density— $\gamma$.

## The Barra et al's Model. A Statistical Mechanical Aspect.

To be more effective in this task, for example, let us explain the statistical mechanics model introduced by Barra's et al (2014) for *social integration* quantifiers as follow. We assign to each person $i$ its own likelihood to marry versus remaining single and for each couple $(i, j)$ too. In the same way, we assign to each person $i$ its individual tendency to have children or not and also for each couple $(i, j)$. These individual and coupling phenomena are then described by individual random variables and couple random variables respectively. It is convenient here to say that the two observations in marriages and births are different: in newborns case, not only couples have this ability to have children but also each individual may have children with different partners even if they have not married. But, in contrast, the monogamy law restricts the marriage cases by not allowing each individual to belong to more than one single couple.

[4] See Barra et al. (2014) for a full account of the model, proofs, and empirical tests.

In mathematical aspect, all these rules convert into topological constraints in the configurational space (such as the *hard-core* interaction of monogamy), or probabilistic constraints (such as the concentration of children per couple around small integers). To do so, assume a given set of points $\{1, \dots, N\}$, and a set of links among the $N$ points as a configuration of marriages $M$ in which there is no points belong to more than one link. Denote singles and married couples by $S_M$ and $C_M$ respectively. Additionally, we call the set of all marriage configurations $\mathcal{M}$. Let us now define a system of configurations in which each configuration has a statistical weight and its partition function created on both individual and couple random variables. Assume $s_i$ is the weight of the person $i$ in the single state and $c_{i,j}$ as the weight of the couple $(i,j)$ in the couple state, and also the partition function of the system is given by

$$Z^{(\mathcal{M})} = \sum_{M \in \mathcal{M}} \prod_{(i.j) \in C_M} \epsilon_{i,j} c_{i,j} \prod_{i \in S_M} s_i,$$

where the binary values $\epsilon_{i,j} \in \{0,1\}$ are the elements of acquaintance matrix of the population and indicate reciprocal knowledge among two individuals. In analogous way, we define a configuration of affiliations $F$ as the set of links among our assumed $N$ points in which the number of children (the links) for each couple $(i,j)$ is distributed according to a *Poisson* distribution $\rho$ of given average $\lambda$. We then denote the individuals without children and the couples with children by $P_F$ (undescended) and $U_F$ (parents) respectively, and the set of all affiliations by $\mathcal{F}$. Now, assume $u_i$ is the weight of the person $i$ in the undescended state and $p_{i,j}$ as the weight of the child $(i,j)$ in the parental state, and also the partition function of the system is given by

$$Z^{(\mathcal{F})} = \sum_{F \in \mathcal{F}} \rho(F) \prod_{(i.j) \in P_F} \epsilon_{i,j} p_{i,j} \prod_{i \in U_F} u_i.$$

In this work, we take the random variables $(c, s, p, u)$ to be constant like the one assumed for the mean field models. Let us define the frequency as $v_M = \frac{K_M}{(N/2)}$ where $K_m$ is the total number of links in the configuration $M$, and the expected value of the marriage frequency that can be calculated as

$$P_{\mathcal{M}} = \mathrm{Av} \frac{\sum_{M \in \mathcal{M}} v_M \prod_{(i,j) \in C_M} \epsilon_{i,j} c_{i,j} \prod_{i \in S_M} s_i}{\sum_{M \in \mathcal{M}} \prod_{(i,j) \in C_M} \epsilon_{i,j} c_{i,j} \prod_{i \in S_M} s_i},$$

where the average operation Av is calculated on the acquaintance matrix ensemble. Analogously, for birth events, we define the frequency $v_F = \frac{K_F}{(N/2)}$ where $K_F$ is the total number of links in the configuration $F$ with its expected value:

$$P_{\mathcal{F}} = \mathrm{Av}\frac{\sum_{F\in\mathcal{F}} v_F \rho(F) \prod_{(i,j)\in P_F} \epsilon_{i,j} p_{i,j} \prod_{i\in U_F} u_i}{\sum_{F\in\mathcal{F}} \rho(F) \prod_{(i,j)\in P_F} \epsilon_{i,j} p_{i,j} \prod_{i\in U_F} u_i}.$$

At this point, we can create our two population system (Immigrant-Native system) in which the single variables $s_i$ and $u_i$ take only two values depending on which population the individual belong to and also the couple variables ($c_{i,j}$ and $p_{i,j}$) take only three values for the three cases $(Imm, Imm)$, $(Nat, Imm)$ and $(Nat, Nat)$. Let us now introduce the following mean-field Hamiltonian in order to include an imitative interaction ($J \geq 0$) between the two populations:

$$H(M) = -J_M \sum_{i\in Nat, j\in Imm} \epsilon_{i,j} \sigma_i \sigma_j \tag{3.1}$$

where

$$\sigma_i = \begin{cases} +1 & \text{if } i \text{ belongs to a mixed marriage} \\ -1 & \text{otherwise,} \end{cases}$$

and in similar fashion, we define

$$H(F) = -J_F \sum_{i\in Nat, j\in Imm} \epsilon_{i,j} \tau_i \tau_j \tag{3.2}$$

where

$$\tau_i = \begin{cases} +1 & \text{if } i \text{ has a child within a mixed couple} \\ -1 & \text{otherwise.} \end{cases}$$

One notes that here the configurations of $\sigma$ and $\tau$ are uniquely determined by monomer-dimer configurations. The partition functions of two models are then given by:

$$Z^{(\mathcal{M})} = \sum_{M\in\mathcal{M}} e^{-H(M)} \prod_{(i.j)\in C_M} \epsilon_{i,j} c_{i,j} \prod_{i\in S_M} s_i,$$

$$Z^{(\mathcal{F})} = \sum_{F\in\mathcal{F}} e^{-H(F)} \rho(F) \prod_{(i.j)\in P_F} \epsilon_{i,j} p_{i,j} \prod_{i\in U_F} u_i.$$

One notices here that the assumption of an exponential Hamiltonian deformation of the monomer-dimer model is a working hypothesis to be tested against experimental data. Let us now define the *frequency of mixed marriages* as $f_M = \frac{M_M}{K_M}$ where $M_M$ is the number of mixed marriages in the configuration $M$, and the expected value of the marriage frequency, that is, the probability of mixed marriages is

$$P_{\mathcal{M}}^{(Nat,Imm)} = \mathrm{Av}\frac{\sum_{M\in\mathcal{M}} f_M e^{-H(M)} \prod_{(i,j)\in C_M} \epsilon_{i,j} c_{i,j} \prod_{i\in S_M} s_i}{\sum_{M\in\mathcal{M}} e^{-H(M)} \prod_{(i,j)\in C_M} \epsilon_{i,j} c_{i,j} \prod_{i\in S_M} s_i}, \tag{3.3}$$

and for newborns with mixed parents we define the *frequency* as $f_F = \frac{M_F}{K_F}$ where $M_F$ is the number of children from mixed couples in the configuration $F$, and its probability is given by

$$P_{\mathcal{F}}^{(Nat,Imm)} = \mathrm{Av}\frac{\sum_{F\in\mathcal{F}} f_F e^{-H(F)} \rho(F) \prod_{(i,j)\in P_F} \epsilon_{i,j} p_{i,j} \prod_{i\in U_F} u_i}{\sum_{F\in\mathcal{F}} \rho(F) \prod_{(i,j)\in P_F} \epsilon_{i,j} p_{i,j} \prod_{i\in U_F} u_i}. \tag{3.4}$$

Hereafter, for simplicity we use $J$ instead of $J_M$ and $J_F$, and $P$ instead of $P_{\mathcal{M}}^{(Nat,Imm)}$ and $P_{\mathcal{F}}^{(Nat,Imm)}$. Recall the monomer dimer pressure $p^{IMD}$ defined by (1.54). For the $P$, Barra et al (2014) found two different results: in the free regime that the monomer-dimer interaction dominates on the interaction $J$ ($J \ll p^{IMD}$), one found for the $P$'s a $\gamma$ dependence of the type $P(\gamma) = r_F\gamma(1-\gamma)$. On the other hand, in the imitative regime when the interaction $J$ dominates on the monomer-dimer interaction (hard core or Poisson) $J \gg p^{IMD}$, they found a functional behavior of the type $P(\gamma) = r_I\sqrt{\gamma(1-\gamma)}$. In these two cases, the constants $r_F$ and $r_I$ depend only on the a priori probabilities of the monomer-dimer interaction.

## Data Description

To build and test our forecasting method, we analyzed a set of unique immigration data drawn from Spanish register data during the period 1999-2010. The significance of this data set is primarily because it was collected in a period when Spain hosted the majority of its immigrant population, and secondly, the fact that this data set contains information of undocumented immigrants who lacked residence permit in that period. The data set includes two types of information: social events and labor market. The data on social events, marriages and births were gathered from *the local offices of Vital Records* and *Spain's National Statistical Agency* (INE) in 735 municipalities which received 85% of Spanish immigrants during the time interval of 1999 to 2008. This social data contain information such as the time of marriage, the place of birth, nationality and municipality of residence. The data on labor contracts which were recorded by *Spain's Continuous Sample of Employment Histories* in the period 2005-2010, consist of information about duration of each contract and its type: temporary or permanent. Social data were disclosed by the municipality of residence for areas with over 10,000 inhabitants, while the data related to labor market were disclosed only for areas with a population greater than 40,000. Primarily, from this data, we identified and extracted classical integration quantifiers on birth and marriage mixed events during 1999-2008 – i.e., parents/partners born abroad. We refer to these quantifiers as *social* (immigrant integration) quantifiers. Next, we extracted information about the number of labor contracts – both temporary and permanent – signed by immigrants in the period of 2005-2010. We refer to these as *socio-economic* (immigrant integration) quantifiers. In our study, we define these quantifiers as a function of immigrant density, $\gamma = \frac{number\ of\ immigrants}{total\ population} \in [0,1]$, in the form:

$$J_p = \frac{the\ numbers\ of\ permanent\ contracts\ given\ to\ immigrants}{the\ numbers\ of\ permanent\ contracts} \tag{3.5}$$

$$J_t = \frac{the\ numbers\ of\ temporary\ contracts\ given\ to\ immigrants}{the\ numbers\ of\ temporary\ contracts} \tag{3.6}$$

$$M_m = \frac{the\ numbers\ of\ mixed\ marriages}{the\ numbers\ of\ marriages} \tag{3.7}$$

$$B_m = \frac{the\ numbers\ of\ newborns\ with\ mixed\ marriages\ parents}{the\ numbers\ of\ newborns} \tag{3.8}$$

## Method and Results

To prepare the data for analysis, we use the following algorithm: we begin by aggregating and cleansing the data in which the records should be checked for missing or incomplete data to avoid inaccuracy in our forecasting approach. After that, data on our quantifiers are organized into two datasets. The first contains information on our social integration quantifiers (see equation (3.7) and

(3.8)). The second set contains data on socio–economic quantifiers (see equation (3.5) and (3.6)). Next, for each data–set, we perform a detailed test of the methodology's forecast performance for increasing intervals of time: period 1 = (2000 to 2001), period 2 = (2000 to 2002), period 3 = (2000 to 2003), etc. The objective is to forecast; 1) the growth law determining the integration process (i.e., establishing whether it is individual independent action or social action that drives the integration process) and 2) the level of integration in the system under study at different time intervals. More precisely, we set out to evaluate the quality of the forecasts in terms of *promptness*—how long is the waiting time before we can correctly identify the growth law for each integration process—*accuracy*—how well the prediction replicates the observed integration value—and finally *robustness*—the forecasting ability of our model over the entire time span.

Starting from data, we extract the growth law of each quantifier in terms of $\Gamma = \gamma(1-\gamma)$[5]. Hereupon, we create a data set for each quantifier per period by merging all the values of Γ with their corresponding integration quantifier values. We then order the data by increasing values of Γ, regardless of their corresponding space and time coordinates. We proceed by grouping the data into bins in terms of Γ, [6] and finally we compute the averages[7]. In order to avoid noisy result, the number of bins is decided after detailed test of different width of bins. The results of these tests reveal that 5 to 15 bins optimize 581–3471 entries on the socio–economic quantifier's data–groups in defined successive intervals, whereas 8 to 30 bins optimize 2421–26546 entries for the datasets on social quantifiers in determined consecutive periods. Moreover, each bin on socio–economic quantifier

---

[5] The control parameter Γ tunes the total number of possible cross-link couplings between immigrant and native populations (see Barra et al. 2014).

[6] For the binning criteria, we used and tested the *constant information* approach. In this approach, the width of the bin will vary over Γ and also there is a constant robustness quality across all bins (Barra et al. 2014).

[7] Since our quantifier values are in the shape of fraction, we compute the averages by using the method of *global mediant*. In the method, the averages are obtained by computing the ratio between the statistical average of nominators and the statistical average of denominators (see Barra et al. 2014).

represents the average values of 65–248 data versus 220–982 data for social indicators as time progresses (for more details see the tables 3.1, 3.2 and appendix A).

**Table 3.1.** Binning and Goodness-of-fit statistics on socio-economic integration quantifiers, Spain 2005–2010.

| **Permanent Jobs** | | | | | | | |
|---|---|---|---|---|---|---|---|
| **Period** | **Total Data** | **The number of bins** | **Population in each bin** | $r_F$ | $R^2_F$ | $r_I$ | $R^2_I$ |
| 1 | 581 | 5 | 116 | 1.507 | 0.9758 | 0.431 | 0.7189 |
| 2 | 1165 | 11 | 106 | 1.555 | 0.9849 | 0.4658 | 0.7498 |
| 3 | 1684 | 12 | 140 | 1.569 | 0.9929 | 0.4896 | 0.7601 |
| 4 | 2279 | 10 | 228 | 1.56 | 0.9899 | 0.4882 | 0.7437 |
| 5 | 2875 | 12 | 240 | 1.515 | 0.9926 | 0.5014 | 0.7645 |
| 6 | 3471 | 14 | 248 | 1.515 | 0.9935 | 0.4988 | 0.7745 |
| **Temporary Jobs** | | | | | | | |
| **Period** | **Total Data** | **The number of bins** | **Population in each bin** | $r_F$ | $R^2_F$ | $r_I$ | $R^2_I$ |
| 1 | 581 | 9 | 65 | 1.8 | 0.9264 | 0.4755 | 0.6574 |
| 2 | 1165 | 12 | 97 | 1.818 | 0.9579 | 0.5376 | 0.6770 |
| 3 | 1684 | 13 | 130 | 1.881 | 0.9596 | 0.5788 | 0.6772 |
| 4 | 2279 | 11 | 207 | 1.887 | 0.9613 | 0.5895 | 0.6809 |
| 5 | 2875 | 13 | 221 | 1.861 | 0.9699 | 0.6059 | 0.6976 |
| 6 | 3471 | 15 | 231 | 1.843 | 0.9770 | 0.6098 | 0.7179 |

**Table 3.2.** Binning and Goodness-of-fit statistics on social integration quantifiers, Spain 1998–2008.

| **Mixed Marriages** | | | | | | | |
|---|---|---|---|---|---|---|---|
| **Period** | **Total Data** | **The number of bins** | **Population in each bin** | $r_F$ | $R^2_F$ | $r_I$ | $R^2_I$ |
| 1 | 2421 | 8 | 303 | 1.242 | 0.6997 | 0.3402 | 0.9767 |
| 2 | 4885 | 11 | 444 | 1.329 | 0.8703 | 0.3725 | 0.9164 |
| 3 | 7432 | 11 | 676 | 1.21 | 0.8591 | 0.3773 | 0.9373 |
| 4 | 10039 | 13 | 772 | 1.077 | 0.8384 | 0.4007 | 0.9757 |
| 5 | 12676 | 15 | 845 | 1.201 | 0.8539 | 0.4223 | 0.9816 |
| 6 | 15334 | 18 | 852 | 1.162 | 0.7977 | 0.4502 | 0.9904 |
| 7 | 18060 | 19 | 951 | 1.156 | 0.8076 | 0.4738 | 0.9882 |
| 8 | 20835 | 23 | 906 | 1.228 | 0.8476 | 0.4865 | 0.9893 |
| 9 | 23649 | 27 | 854 | 1.215 | 0.8512 | 0.5009 | 0.993 |
| 10 | 26546 | 28 | 941 | 1.187 | 0.8583 | 0.5242 | 0.9931 |
| **Newborns** | | | | | | | |
| **Period** | **Total Data** | **The number of bins** | **Population in each bin** | $r_F$ | $R^2_F$ | $r_I$ | $R^2_I$ |
| 1 | 2421 | 11 | 220 | 0.8164 | 0.9272 | 0.3099 | 0.9637 |
| 2 | 4885 | 14 | 349 | 0.8595 | 0.9522 | 0.319 | 0.9615 |
| 3 | 7432 | 18 | 411 | 0.8167 | 0.9469 | 0.3333 | 0.9616 |
| 4 | 10039 | 19 | 523 | 0.7761 | 0.8874 | 0.3027 | 0.9772 |
| 5 | 12676 | 21 | 582 | 0.8067 | 0.9008 | 0.3012 | 0.9778 |
| 6 | 15334 | 23 | 659 | 0.7239 | 0.7857 | 0.2823 | 0.9731 |
| 7 | 18060 | 27 | 667 | 0.6895 | 0.7746 | 0.2828 | 0.9794 |
| 8 | 20835 | 30 | 690 | 0.6791 | 0.7826 | 0.2812 | 0.98 |
| 9 | 23649 | 30 | 780 | 0.6702 | 0.7906 | 0.2809 | 0.9803 |
| 10 | 26546 | 27 | 982 | 0.6484 | 0.8114 | 0.2831 | 0.9883 |

The growth law of the integration process can then be expressed over the specified periods mathematically by using curve fitting tools over the obtained bins. The curve fitting process reveal that the data set on socio–economic quantifiers can be well predicted by linear model $r_F\Gamma$ while the nonlinear model $r_I\sqrt{\Gamma}$ successfully projects the social data–set across the analyzed time sequences. Hence our results agree with those reported by Barra et al. (2014). Thereafter, for simplicity of notation, we use $r$ instead of both $r_F$ and $r_I$. These findings shows that the values of coefficient $r$ recorded over the indicated periods converge to a fixed number $\tilde{r}$ and determine a curve which holds the formula:

$$r(t) = \tilde{r}\left(1 \pm e^{-\frac{t}{K}}\right), t = 2, \dots, t_f \tag{3.9}$$

where $t_f$ is referring to the final period and the $\tilde{r}$ and $K$ are parameter estimates describing the growth law using information from previous time periods (see tables 3.3 and 3.4).

**Table 3.3.** Forecasting measures for socio-economic integration quantifiers, Spain 2005–2010.

| **Permanent Jobs** | | | |
|---|---|---|---|
| **Period** | ***r*** | ***r̃*** | ***K*** |
| 1 | 1.507 (1.410, 2.472) | ------------------------ | --------- |
| 2 | 1.555 (1.469, 1.642) | 1.507 (1.410, 2.472) | 0.0000 |
| 3 | 1.569 (1.501, 1.637) | 1.555 (1.469, 1.642) | 0.0000 |
| 4 | 1.56 (1.49, 1.63) | 1.569 (1.501, 1.637) | 0.0000 |
| 5 | 1.515 (1.468, 1.563) | 1.56 (1.49, 1.63) | 0.0000 |
| 6 | 1.515 (1.476, 1.554) | 1.515 (1.468, 1.563) | 0.0000 |
| **Temporary Jobs** | | | |
| **Period** | ***r*** | ***r̃*** | ***K*** |
| 1 | 1.8 (1.514, 2.086) | ------------------------ | --------- |
| 2 | 1.818 (1.629, 2.007) | 1.8 (1.514, 2.086) | 0.0000 |
| 3 | 1.881 (1.66, 2.102) | 1.818 (1.629, 2.007) | 0.0000 |
| 4 | 1.887 (1.703, 2.071) | 1.881 (1.66, 2.102) | 0.0000 |
| 5 | 1.861 (1.732, 1.99) | 1.887 (1.703, 2.071) | 0.0000 |
| 6 | 1.843 (1.735, 1.951) | 1.861 (1.732, 1.99) | 0.0000 |

**Table 3.4.** Forecasting measures for social integration quantifiers, Spain 1998–2008.

| Mixed Marriages | | | |
|---|---|---|---|
| **Period** | $r$ | $\tilde{r}$ | $K$ |
| 1 | 0.3402 (0.2973, 0.3831) | --------------------------- | --------------------------- |
| 2 | 0.3725 (0.3017, 0.4432) | 0.3759 | 0.4247 |
| 3 | 0.3773 (0.3214, 0.4333) | 0.377 (0.3658, 0.3881) | 0.4303 (0.3383, 0.5222) |
| 4 | 0.4007 (0.3644, 0.4369) | 0.3865 (0.3504, 0.4227) | 0.4824 (0.1587, 0.806) |
| 5 | 0.4223 (0.3927, 0.452) | 0.3976 (0.3618, 0.4334) | 0.5452 (0.2018, 0.8886) |
| 6 | 0.4502 (0.4296, 0.4708) | 0.4111 (0.3711, 0.451) | 0.6267 (0.2191, 1.034) |
| 7 | 0.4738 (0.4509, 0.4967) | 0.4254 (0.3829, 0.4679) | 0.7269 (0.263, 1.191) |
| 8 | 0.4865 (0.4647, 0.5084) | 0.438 (0.3961, 0.4799) | 0.8266 (0.3347, 1.318) |
| 9 | 0.5009 (0.4835, 0.5183) | 0.4497 (0.4086, 0.4908) | 0.9287 (0.4107, 1.447) |
| 10 | 0.5242 (0.5066, 0.5418) | 0.4631 (0.4211, 0.5051) | 1.064 (0.4949, 1.634) |
| **Newborns** | | | |
| **Period** | $r$ | $\tilde{r}$ | $K$ |
| 1 | 0.3099 (0.27, 0.3498) | --------------------------- | --------------------------- |
| 2 | 0.319 (0.2852, 0.3528) | 0.3145 | 0.2686 |
| 3 | 0.3333 (0.298, 0.3686) | 0.3207 (0.1708, 0.4706) | 0.07791 (−1844, 1844) |
| 4 | 0.3027 (0.2791, 0.3263) | 0.3162 (0.2815, 0.351) | 0.03235 |
| 5 | 0.3012 (0.2794, 0.323) | 0.3132 (0.2914, 0.335) | 0.02362 |
| 6 | 0.2823 (0.2611, 0.3036) | 0.3076 (0.2836, 0.3317) | 0.208 (−0.8099, 1.226) |
| 7 | 0.2828 (0.2659, 0.2997) | 0.3034 (0.2822, 0.3246) | 0.2693 (−0.2819, 0.8205) |
| 8 | 0.2812 (0.2657, 0.2967) | 0.3001 (0.2812, 0.3189) | 0.3059 (−0.1312, 0.7431) |
| 9 | 0.2809 (0.2655, 0.2963) | 0.2975 (0.2807, 0.3143) | 0.3332 (−0.04511, 0.7115) |
| 10 | 0.2831 (0.2704, 0.2958) | 0.2958 (0.2809, 0.3107) | 0.3518 (0.01316, 0.6905) |

Based on this piece of evidence, we suggest the parameter $\tilde{r}$ as a predictor to estimate the coefficient $r$ of subsequent period. Thereafter, we insert the predictor of $r$ into our models, and proceed by predicting the future outcomes. Our aim is to predict the quantifier values for new observations given their immigrant densities. It is worth noticing that in our approach, the value of each integration quantifier in the coming years also considers the new immigrants density $\Delta\gamma$ and thus the new value becomes $Q_i(\Gamma) + Q_i(\Delta\Gamma), i = 1,2,3,4$; where $Q$ represents the extracted growth law function for each quantifier and $\Delta\Gamma = \Delta\gamma(1 - \Delta\gamma)$.

For instance, regarding equation (3.9), assuming that the reported values of "$r$" through all these periods of time is a series of numbers, "$r$" will converge to the fixed numbers 0.5212 & 0.2821 for the mixed marriages and births with mixed parents quantifiers and numbers 1.515 & 1.861 for the quantifiers measuring the coefficient numbers of permanent and temporary jobs market respectively. Thus, if we use these "$r(t)$" values as the set of points that determines the curve for the four quantifiers, the following formulas apply:

$$r_{J_p}(t) = \tilde{r}_{J_p}\left(1 \pm e^{-\frac{t}{K_{J_p}}}\right) \quad \tilde{r}_{J_p} = 1.515, K_{J_p} = 0.0000$$

$$r_{J_t}(t) = \tilde{r}_{J_t}\left(1 \pm e^{-\frac{t}{K_{J_t}}}\right) \quad \tilde{r}_{J_t} = 1.861, K_{J_t} = 0.0000$$

$$r_{M_m}(t) = \tilde{r}_{M_m}\left(1 - e^{-\frac{t}{K_{M_m}}}\right) \quad \tilde{r}_{M_m} = 0.5212, K_{M_m} = 0.05221$$

$$r_{B_m}(t) = \tilde{r}_{B_m}\left(1 + e^{-\frac{t}{K_{B_m}}}\right) \quad \tilde{r}_{B_m} = 0.2821, K_{B_m} = 0.1058$$

where $t = 1, \dots, t_f$. As a result, the values at convergence are introduced into our models for predicting future outcomes:

$$J_p(\Gamma) = 1.515\Gamma \qquad for\ \ Permanent\ contracts$$
$$J_t(\Gamma) = 1.861\Gamma \qquad for\ Temporary\ contracts$$

$$M_m(\Gamma) = 0.5212\sqrt{\Gamma} \qquad for\ \ Mixed\ marriages$$
$$B_m(\Gamma) = 0.2821\sqrt{\Gamma} \quad for\ Newborns\ with\ mixed\ parents$$

The quality of the subsequent forecasts turns out to be prompt, accurate and robust. Figure 3.1 illustrates how the goodness of fit of our forecasts changes as we progressively add information from subsequent time periods. As shown in the figure 3.1, this curve fitting exercise tells us the growth law that provides the best fit, when the entire set of data is considered, visibly delivers substantially better forecasts as early on as from period one. Even in the worst case scenario (see upper right panel in the figure 3.1) the forecast obtained by applying the square root growth law deliver more efficient estimates than the linear growth law already from period two and beyond. Thus, the predictability with respect to discerning the underlying mechanism for integration is prompt since the correct behavior emerges from the dataset as early as the first year, and no later than after two years.

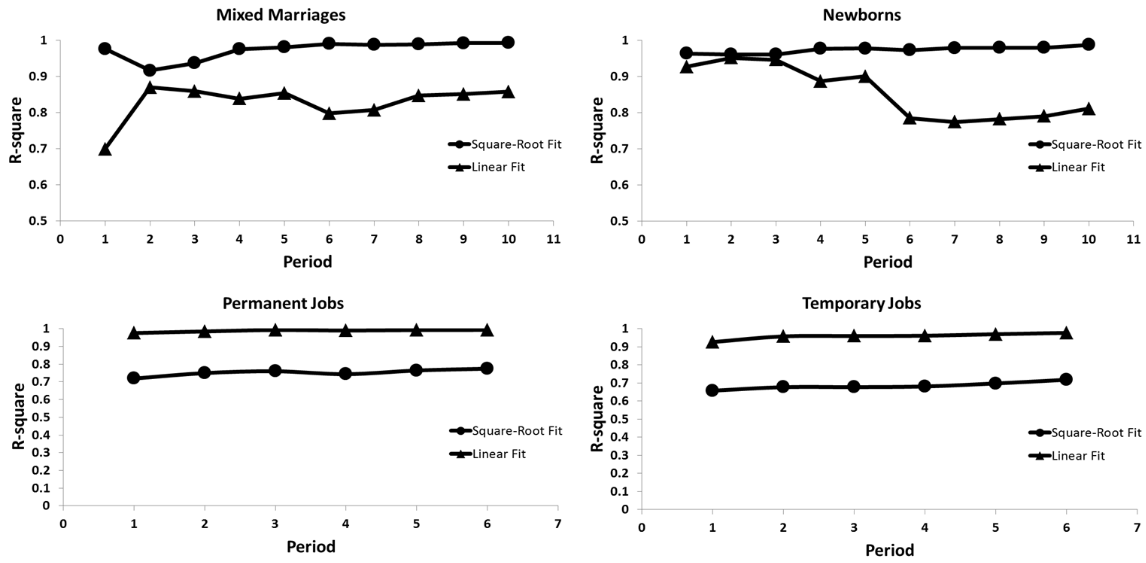


**Figure 3.1.** Here each circular bullet displays the coefficient of determination computed for square–root fitting $r_I\sqrt{\Gamma}$ in the relevant period and each triangular bullet represents the analogous value recorded for linear model $r_F\Gamma$.

Figure 3.2 shows how the forecasted values $\tilde{r}$ (grey points) based on past data match the values $r$ observed in the successive year. The match turns out to be very accurate. The Adjusted Mean Absolute Percentage Errors[8] are within 1%.

[8] We used the Adjusted Mean Absolute Percentage Error which is a valid quantity to show the accuracy of the predictions:

adjusted MAPE $= \frac{1}{n}\sum_{t=1}^{n}\frac{|f_t - y_t|}{(f_t + y_t)/2}$ where $y_t$ and $f_t$ are observed and forecasting values respectively (see Armstrong 1985).

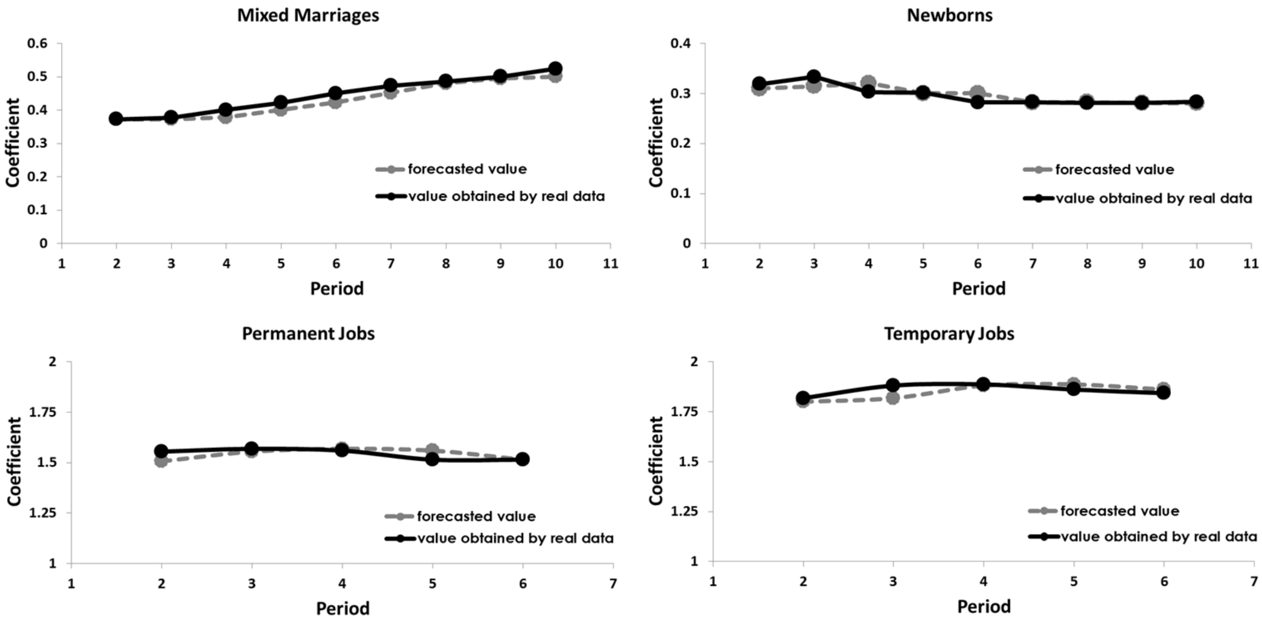


**Figure 3.2.** The black points represent the value of the coefficient $r$ (for the suitable growth law identified in figure 3.1) obtained by real data collected up to the indicated year, grey points represent the forecasted value of the same coefficient obtained with the equation (3.9) – the Adjusted Mean Absolute Percentage Errors do are always under 1%.

Figure 3.3, finally, analyzes the robustness of the forecasting ability with respect to identified models over the entire time span. The fit of the forecasted value vis–a–vis the observed value remain at an exceptionally high level also for large time intervals. The integration quantifiers exhibiting linear growth behavior are identified with high accuracy, with an $R^2$ that never goes below .98 in the case of permanent contracts and .94 for temporary contracts.[9] As for the two quantifiers evolving like the square root, the lowest $R^2$ is .91 for Mixed marriages, whereas in the case of newborns with mixed parents it is .95.

[9] $R^2$ indicates how well the observed outcomes are replicated by the statistical model. The measure ranges from 0 to 1 such that the larger numbers representing better fits and also 1 indicates a perfect fit:

$$R^2 = 1 - \frac{\sum_{t=1}^{n}(y_t - f_t)^2}{(y_t - \bar{y})^2}$$

where $y_1, \dots, y_n$ are the observed values, $f_1, \dots, f$ are the forecasts, and $\bar{y}$ is the average of the data (Draper and Smith 1998).

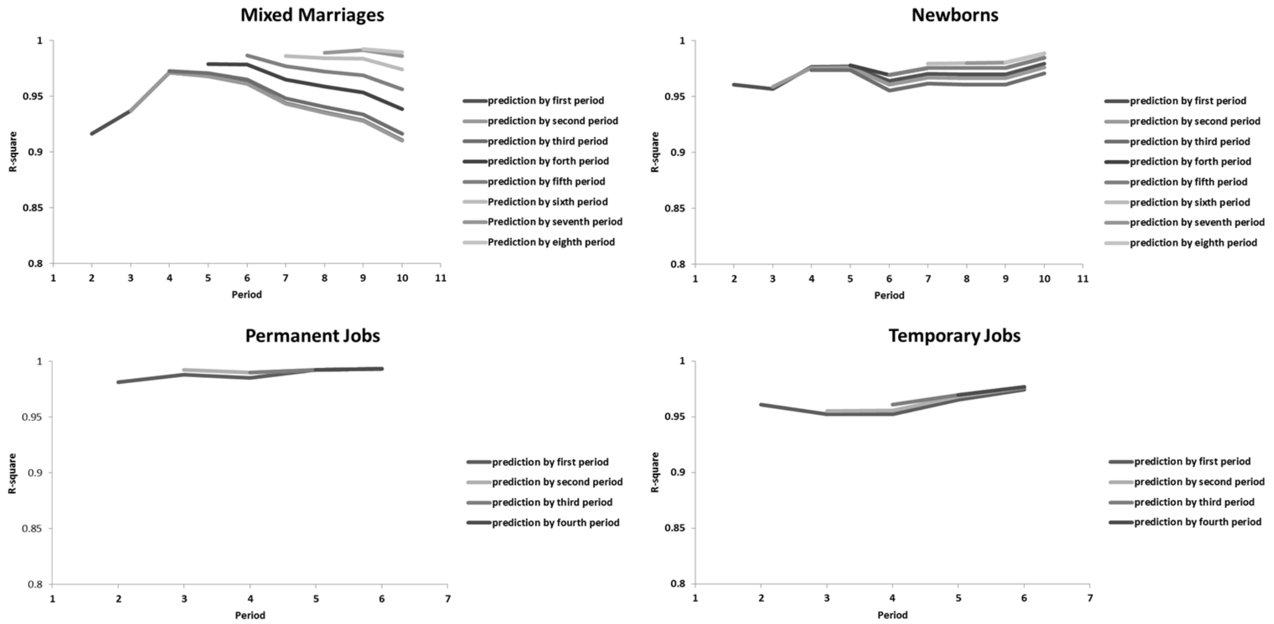


**Figure 3.3.** Forecasts by the equation (3.9) are tested by the $R^2$ coefficient against real data at increasing time intervals. $R^2$ never goes below .91 even for forecasts 9 years ahead.

## Concluding discussion

The main objective of this work was to propose a quantitative method capable of elaborating precise forecasts of immigrant integration as a function of immigrant density. This objective has been accomplished.

The forecasting ability of the proposed model turns out to be prompt, accurate and robust. *Promptnes*s is found since the applied method successfully determines and differentiates between integration processes sensitive to social interaction or not, at very early stages (maximum two time periods). *Accuracy* and *Robustness* is found since, once we have determined the growth law, our prediction algorithm provide very accurate forecasts over the entire time sequence. Hence, using this framework it is possible to estimate the future rate of, for example, inter–marriage, if the size of the immigrant population rise by say 2–3%.

An important quality of our forecasting framework is that it is capable of uncovering the underlying mechanism driving the integration process—social interaction or independent decision making—at an early stage in the immigration cycle. The capacity to foretell information of this type is by no means trivial since the two mechanisms are likely to demand different policy responses. For example, when integration grow linearly with immigrant density, as our labor participation indicators, effective policy responses should focus on problems such as access to labor markets, to improve integration, whereas integration induced by social action and interaction requires policies targeting the quality and intensity of interaction between immigrants and locals.

Our findings are of particular value to governments and researchers engaged in formulating more effective and precise immigration and integration policies. It is also an excellent research tool for scholars interested in explaining individual integration outcomes since it unveils in a general but powerful way the presence or absence of social network effects in integration phenomena.

# References

Alba, R. and Nee, V. 1997. Rethinking assimilation theory for a new era of immigration. *International migration review*, 31(4):826–74.

Alberici, D. Contucci, P. and Mingione E. 2014. A mean-field monomer-dimer model with attractive interaction: exact solution and rigorous results. *Journal of mathematical physics*, 55(6).

Andramonov, M. Rubinov, A. and Glover B. 1999. Cutting Angle Methods in Global Optimization, *Applied Mathematics Letters*, 12(13), Elsevier Science Ltd.

Armstrong, J. S. 1985. *Long–range forecasting: from crystal ball to computer*. Wiley, 2nd edition.

Ballerini M, Cabibbo N, Candelier R, Cavagna A, Cisbani E, Giardina I, Lecomte V, Orlandi A, Parisi G, Procaccini A, Viale M and Zdravkovic V. (2008). Interaction ruling animal collective behavior depends on topological rather than metric distance: Evidence from a field study, *Proc. Natl. Aca. Sc.*, 105, 1232–1237.

Barra A. and Contucci, P. 2010. Toward a quantitative approach to migrants social integration. *EPL (Europhysics Letters),* 89 (6), 68001.

Barra A., Contucci, P., Sandell, R. and Vernia, C. 2014. An analysis of a large dataset on immigrant integration in Spain. The statistical mechanics perspective on social action. *Scientific Reports* 4, 4174.

Bialek, W., Cavagna, A., Giardina, I., Mora, T., Silvestri, E., Viale, M. and Walczak A.M. 2012. Statistical mechanics for natural flocks of birds. *Proc. Natl. Acad. Sc.*, 109, 4786–4791.

Bianchi, A., Contucci, P. and Giardina, C. 2004. Thermodynamic limit for mean field spin models, Mathematical Physics Electronic Journal, 9(6), 1-15.

Blau, P.M., Blum, T.C. and Schwartz, J.E. 1982. Heterogeneity and Inter–marriage. *American Sociological Review*. 47(1), 45–62.

Blau, P.M., Beeker, C. and Fitzpatrick, K.M. 1984. Intersecting social affiliations and inter–marriage. *Social Forces*, 62(3), 585–606.

Bouchaud, J.P. and Potters, M. 2004. *Theory of financial risks: from statistical physics to risk managemenent*. Oxford University Press.

Brent, R. P. 1973. *Chapter 4: an algorithm with guaranteed convergence for finding a zero of a function, algorithms for minimization without derivatives*, Englewood Cliffs, NJ: Prentice-Hall.

Brock, W. and Durlauf, S.N. 2001. Discrete choice with social interactions, *The Review of Economic Studies*, 68(2), 235–260.

Canada Government. 2012. Canada's economic action plan (2012), *a fast and flexible economic immigration system, jobs growth and long–term prosperity*. Technical report, Government of Canada.

Castellano, C., Marsili, M. and Vespignani, A. 2000. Nonequilibrium phase transition in a model for social influence. *Physicl Review Letters*, 85(6), 3536.

Castles, S. and Miller, M. J. (eds) 2009. *The age of migration – International population movements in the modern world*, Pallgrave McMillian, New York.

Christodoulos, A. A. and Panos, M. P. 2008. *Encyclopedia of Optimization*, Springer Science and Business Media.

Conn, A. R., Gould N. I. M. and Toint P. L. 2000. *Trust region methods*, Society for industrial and applied mathematics.

Contucci, P., Gallo, I. and Menconi, G. 2008. Phase transitions in social sciences: two–populations mean field theory, *International Journal of Modern Physics B*. 22(14). P 1–14.

Contucci P, and Giardina, C. 2008. Mathematics and Social Sciences: A statistical mechanics approach to immigration. *ERCIM News*. 73, 8241.

Cortina, C. T., Esteve, A. and Domingo, A. 2008. Marriage patterns of the foreign-born population in a new country of immigration: The case of Spain1. *International Migration Review*, 42(4), 877–902.

Curie, P. 1895. Propriete ferromagnetique des corps a diverse temperatuires, *ann. de chim. et d phys.*, 7e serie, v, 289, Ghirlanda.

Dekker, T. J. 1969. Finding a zero by means of successive linear interpolation, *in Dejon, B.; Henrici, P., Constructive Aspects of the Fundamental Theorem of Algebra, London: Wiley-Interscience*.

Draper, N. R. and Smith, H. 1998. *Applied Regression Analysis*. Wiley–Interscience.

European Commission. 2005. *A common agenda for integration framework for the integration of third–Country nationals in the European Union*. Technical Report COM (389), Commission of the European Communities,

European Commission. 2010. *EUROPE 2020: A strategy for smart, sustainable and inclusive growth*. COM (2020).

European Commission. 2011. *The global approach to migration and mobility*. EU Report, Technical Report COM(743).Sec(1353).

European Commission. 2014. *EU actions to make integration work: Common basic principles, European Website on Integration*, Technical report.

European Council. 2010. *The stockholm programme–an open and secure europe serving and protecting citizens official journal*, Technical Report C(115/1–38).

Fedele, M. 2011. *A mean field model for the collective behavior of interacting multi-species particles: mathematical results and application to the inverse problem*, PhD Thesis, Mathematics Department, Universita di Bologna.

Galam, S., Yokoi, C.S.O., and Salinas, S.R. 1998. Metamagnets in uniform and random fields, *Physical Review B*, 57(14), 8370-8374.

Gallo, I., Barra, A. and Contucci, P. 2009. Parameter evaluation of a simple mean–field model of social interaction. *Math. Models Methods Appl. Sci*. 19, 1427.

Gallo, I., and Contucci, P. 2008. Bipartite mean field spin systems. Existence and solution. *Math. Phys. Electron. J.*, 14.

Giovagnoli, M. 2011. *Improving the naturalization process: Better immigrant integration lead to economic growth*. Immigration Policy Center, American Immigration Council.

Gordon, M.M. 1964. *Asimilation in American Life: The role of Race, Religion, and National Origins*. Oxford University Press. New York

Granovetter, M. 1974. *Getting a Job: A study of contacts and careers*. The University of Chicago Press. Chicago.

Guerra, F. 2005. Mathematical aspects of mean field spin glass theory, *4ECM Stockholm 2004, European mathematical society*, 719-732.

Heilmann, O.J. and Lieb, E.H. 1970. Monomers and dimers, *Physical Review Letters*, 24, 1412–1414.

Heilmann O.J. and Lieb E.H. 1972. Theory of monomer-dimer systems, *Commun. Math. Phys.* 25, 190-232.

Heilmann O.J. and Lieb E.H. 1979. Lattice models for liquid crystals, *J. Stat. Phys.*, 20, 680-693.

Hwang, S.S., Saenz, R. and Aguirre, B.E. 1997. Structural and assimilationist explanations of Asian American inter–marriage. *Journal of Marriage and the Family*, 59(3), 758–72.

IOM. 2011. *International dialogue on migration N. 17 – Migration and social change*. The International Dialogue on Migration Red Book Series, Geneva, Switzerland.

Jacoby T. Culver C., Daley R.M. and Munana C. 2013. *US economic competitiveness at risk: A midwest call to action on immigration reform*. The Chicago Council on Global Affairs, Chicago, Illinois.

Kalmijn, M. 1998. Inter–marriage and Homogamy: Causes, Patterns, Trends. *Annual review of sociology* 24(24), 395–421.

Kincaid, J. M. and Cohen, E. G. D. 1975. Phase diagrams of liquid helium mixtures and metamagnets: experiment and mean field theory, *Physics Reports*, 22(2), 57-143.

Kochmanski, M. Paszkiewicz, T. and Wolski, S. 2013. Curie-Weiss magnet a simple model of phase transition, *European Journal of Physics*, 34(6).

Kulske, C. and Le Ny, A. 2007. Spin-flip dynamics of the Curie-Weiss model: Loss of Gibbsianness with possibly broken symmetry, *Communications in Mathematical Physics*, 271(2), 431-454.

Levy M. 2005. Social phase transition. *Journal of Economic Behavior & Organization*, 57. 71–87.

Mantegna, R.N. and Stanley, H.E. 1999. *Introduction to econophysics: correlations and complexity in finance*. Cambridge University Press.

McFadden, D. 2001. Economic choices, *The Amer. Econ. Rev*., 91, 351–378.

Motizuki, K. 1959. Metamagnetism of methylamine chrome alum, *Journal of the Physical Society of Japan*, 14(6), 759-771.

Niessen J. and Huddleston T. (eds) 2010. *Handbook on integration for policy–makers and practitioners*. Migration Policy Group on behalf of the European Commission, Farance.

Penninx R., Spencer, D. and Hear, N.V. 2008. *Migration and integration in Europe: The state of research*. ESRC Centre on Migration, Policy and Society (COMPAS) University of Oxford.

Portes, A. and M. Zhou. 1993. The new second generation: Segmented assimilation and its variants. *The Annals of the American Academy of Political and Social Science*, 530.

Qian, Z., Glick, J.E., and Batson, C.D. 2012. Crossing boundaries: Nativity, Ethnicity, and Mate Selection. *Demography*, 49(2), 651–75.

Raijman R., and Tienda. M. 1999. Immigrants socio–economic progress post–1965: forgingmobility or survival? In *The Handbook of International Migration*. Russell Sage Foundation, New York.

Rubinov, A. 2000. *Abstract convexity and global optimization. Nonconvex Optimization and its Aplications*, kluwer academic publishers.

Seyedi, S.A. 2010. *The Cutting Angle Method for Optimal Control Problems*, Master Thesis, Universiti Teknologi Malaysia .

Stanley. H.E. 2008. Econophysics and the current economic turmoil. *American Physical Society News*, 11(17):8.

Stevens, G. and Swicegood, G. 1987. The linguistic context of ethnic endogamy. *American Sociological Review*, 52(1):73–82. Retrieved from http://www.jstor.org/stable/2095393

Talagrand, M. 2003. *Spin glasses: a challenge for mathematicians: cavity and mean field models*, Springer Verlag.

Thompson, C.J. 1988. *Classical equilibrium statistical mechanics*, Clarendon Press.

Van Tubergen. F. 2006. *Immigrant integration: A cross–national study*. LFB Scholarly Publishing LLC.

Van Tubergen F. and Maas. I. 2007. Ethnic inter–marriage among immigrants in the Netherlands: An analysis of population data. *Social Science Research*, 36(3):106586.

Watts, D. J. and Strogatz, S. H. 1998. Collective dynamics of small–world networks. *Nature*, 393 (6684), 440–442.

Weber, M. 1978. *Economy and Society: An outline of interpretive sociology*. University of California Press., 23.

Weiss, P. 1907, L'hypothes du champ moleculaire e la propriete ferromagnetique, *Journal of Physics*, 4e serie, VI, 661.

Yeomans, J. M. 1992. *Statistical Mechanics of Phase Transitions*, Oxford University Press.

# Appendix A

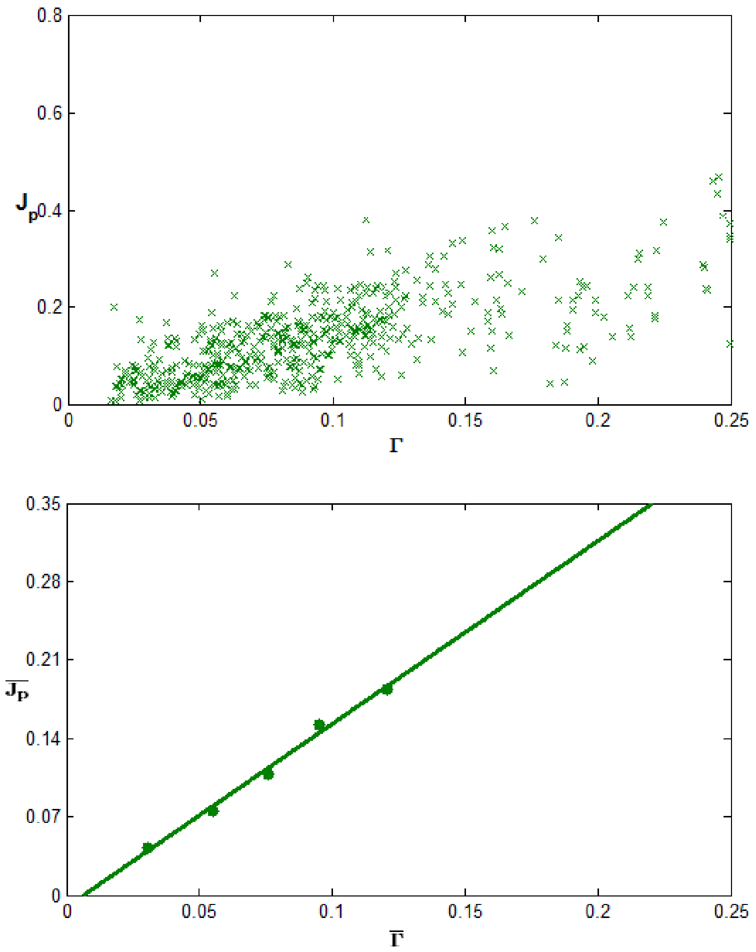


**Figure 4.1** Raw data and average behavior of permanent jobs quantifier in period 1.

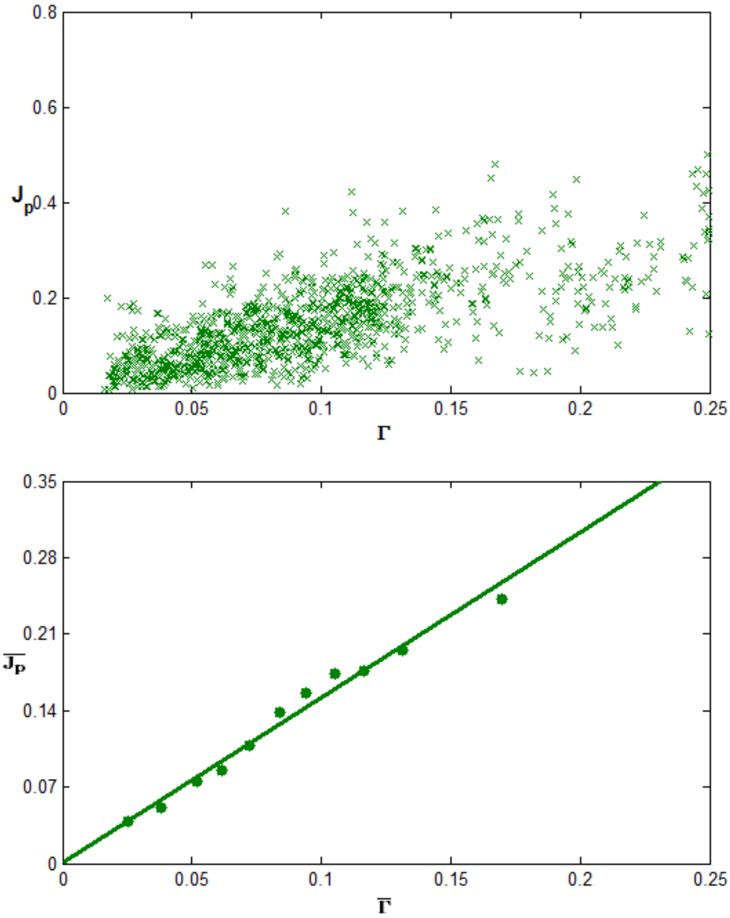


**Figure 4.2** Raw data and average behavior of permanent jobs quantifier in period 2.

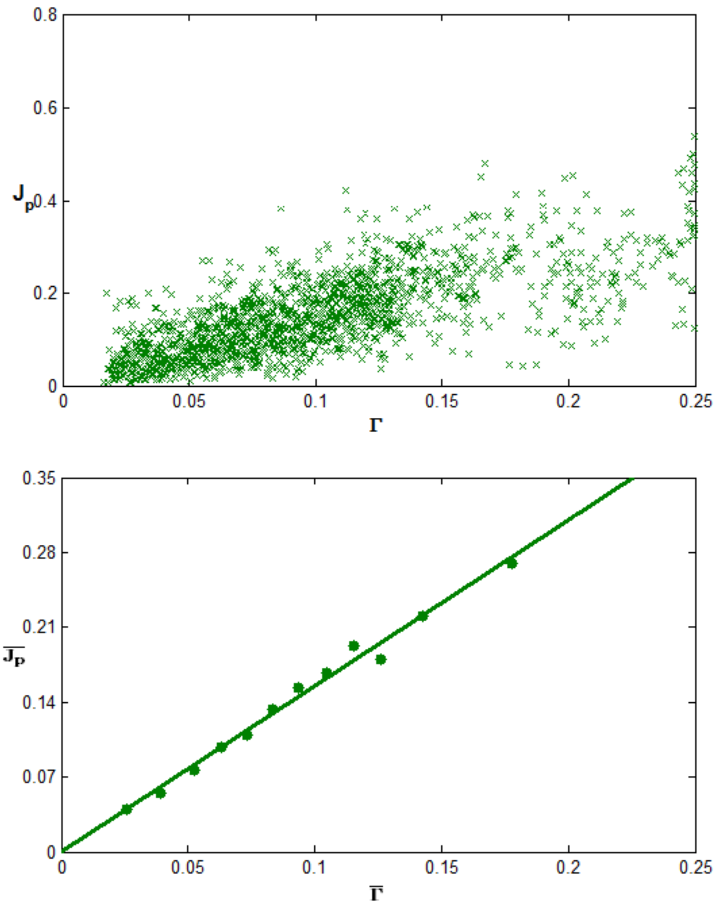


**Figure 4.3** Raw data and average behavior of permanent jobs quantifier in period 3.

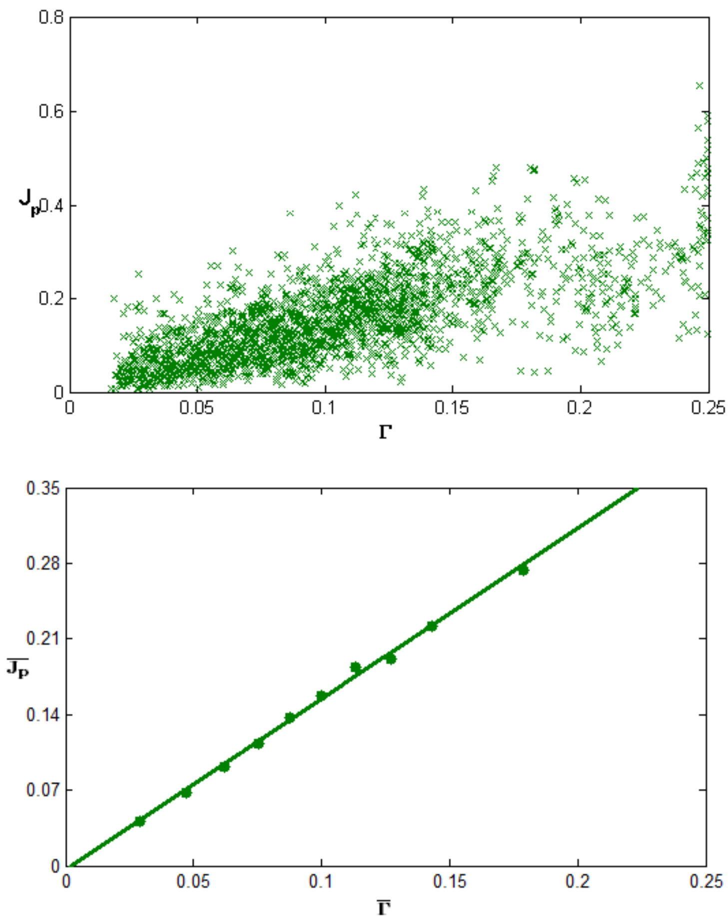


**Figure 4.4** Raw data and average behavior of permanent jobs quantifier in period 4.

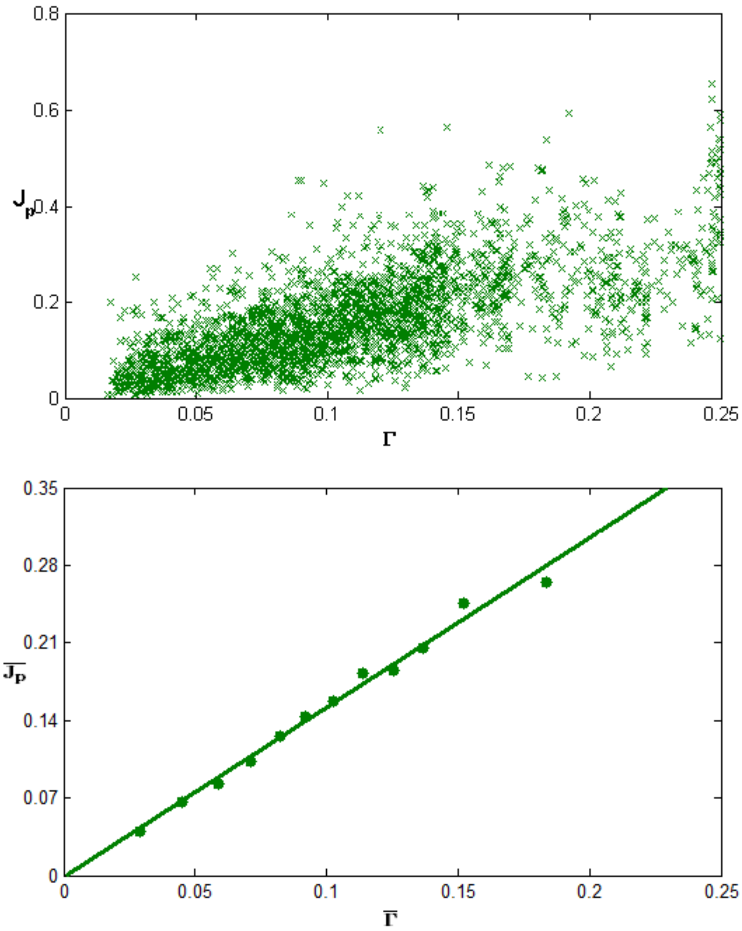


**Figure 4.5** Raw data and average behavior of permanent jobs quantifier in period 5.

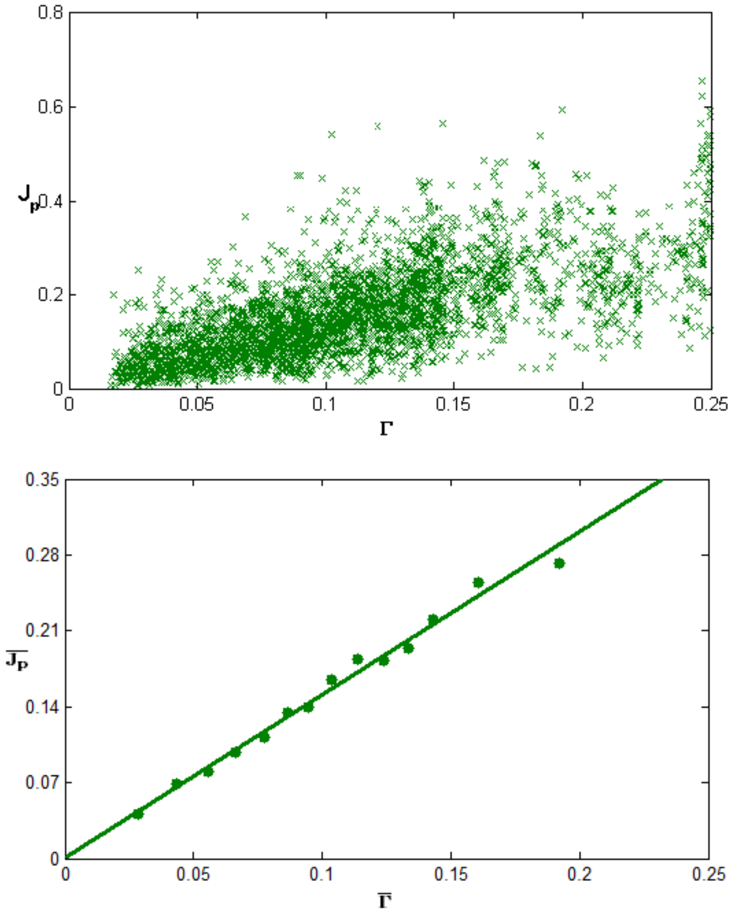


**Figure 4.6** Raw data and average behavior of permanent jobs quantifier in period 6.

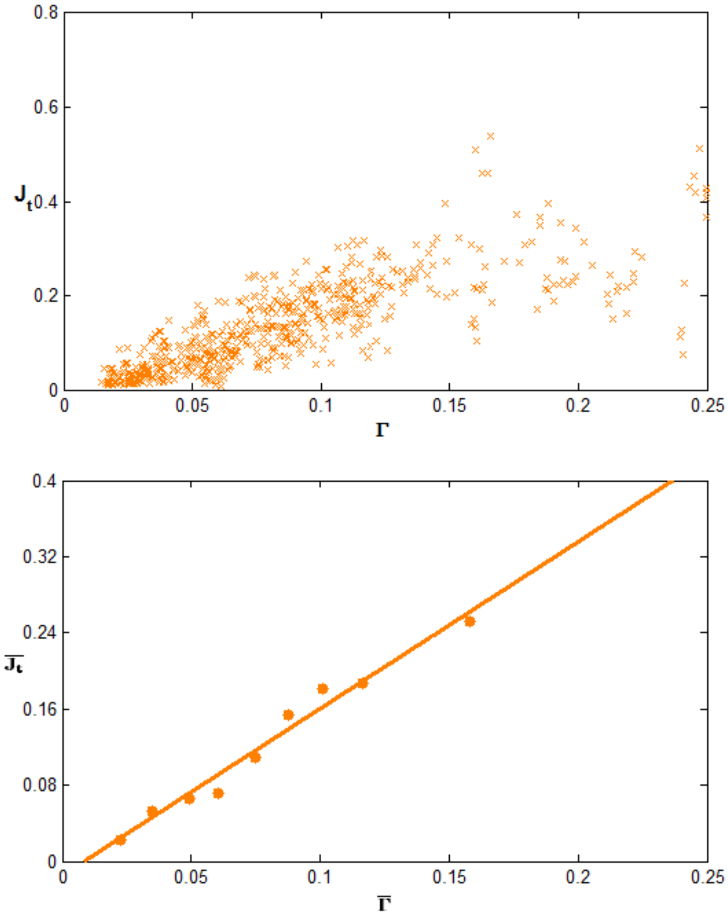


**Figure 4.7** Raw data and average behavior of temporary jobs quantifier in period 1.

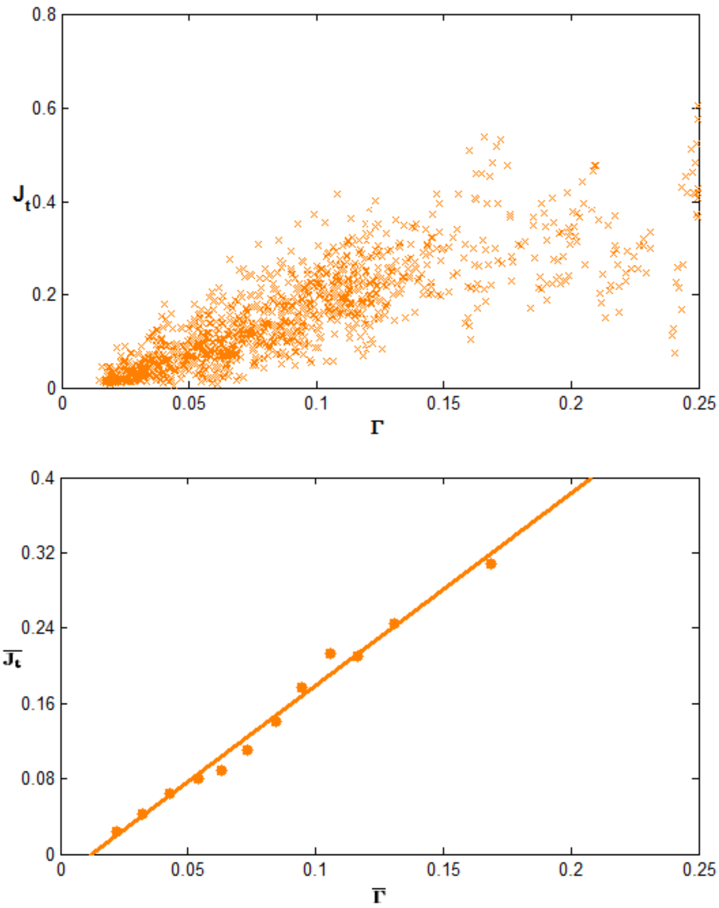


**Figure 4.8** Raw data and average behavior of temporary jobs quantifier in period 2.

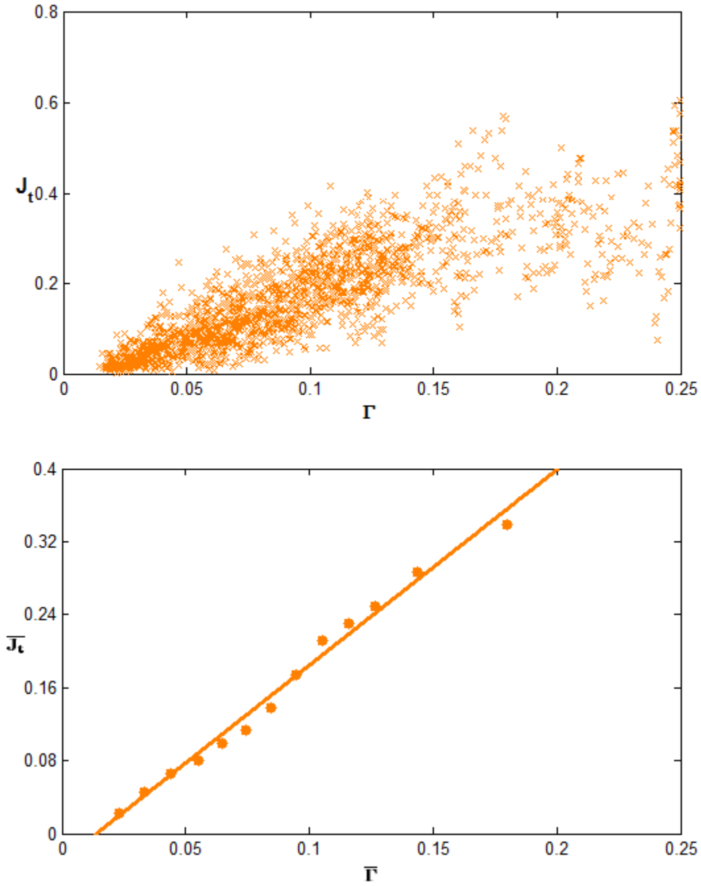


**Figure 4.9** Raw data and average behavior of temporary jobs quantifier in period 3.

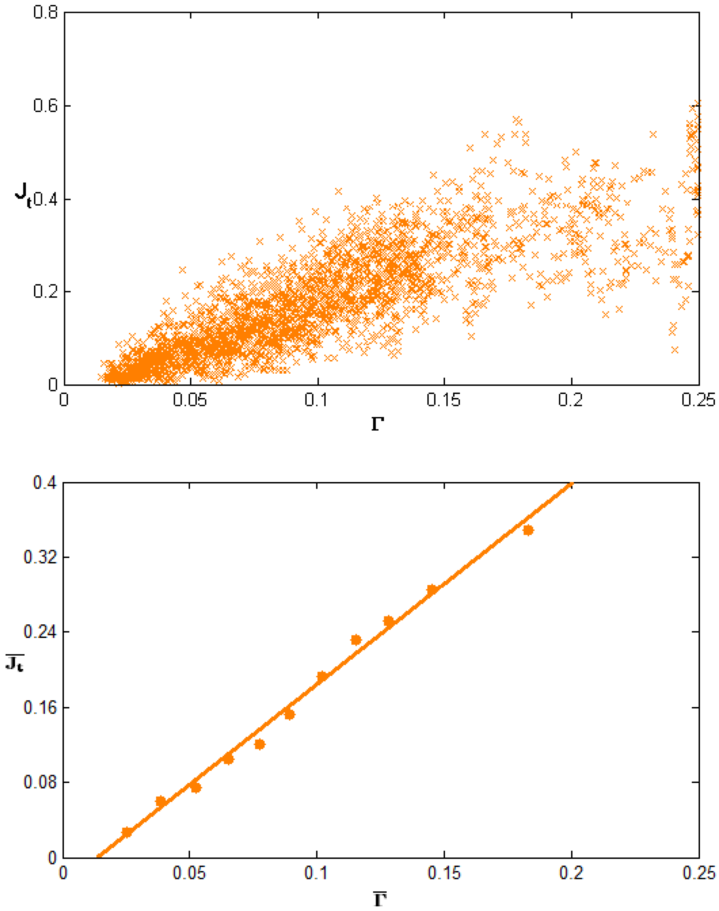


**Figure 4.10** Raw data and average behavior of temporary jobs quantifier in period 4.

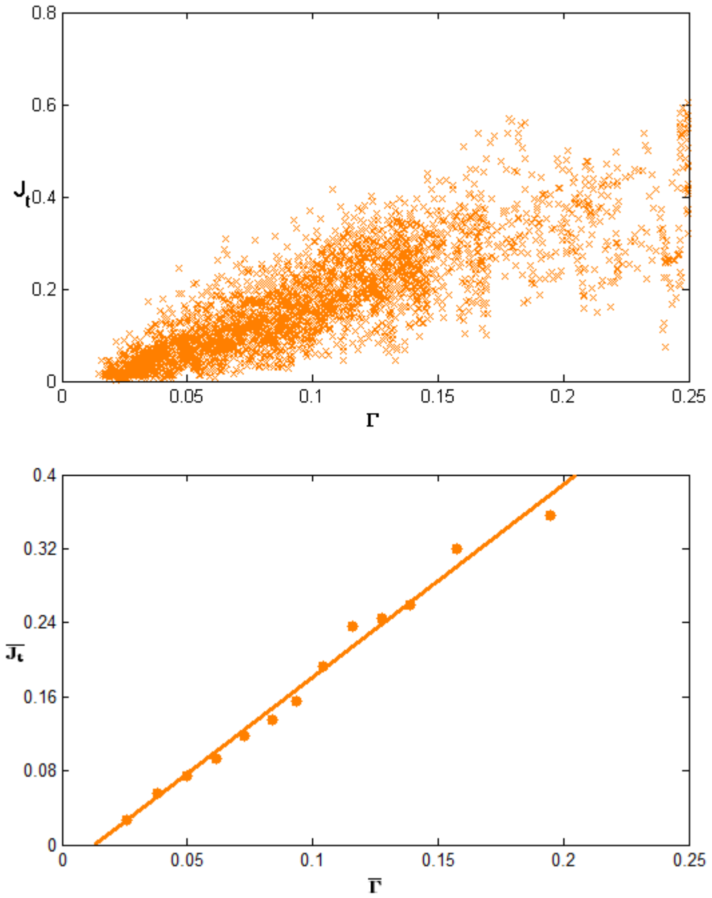


**Figure 4.11** Raw data and average behavior of temporary jobs quantifier in period 5.

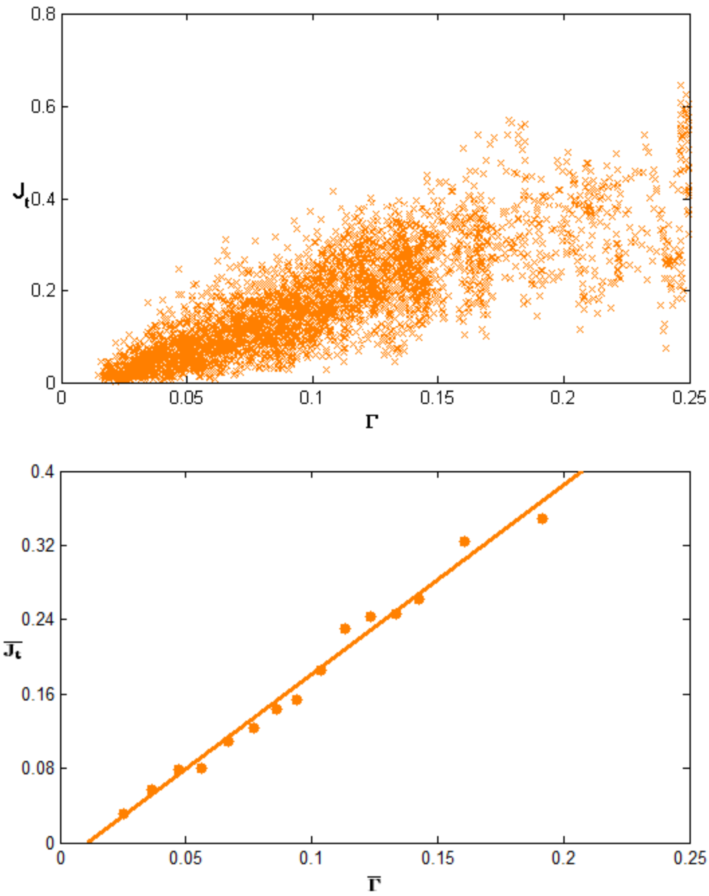


**Figure 4.12** Raw data and average behavior of temporary jobs quantifier in period 6.

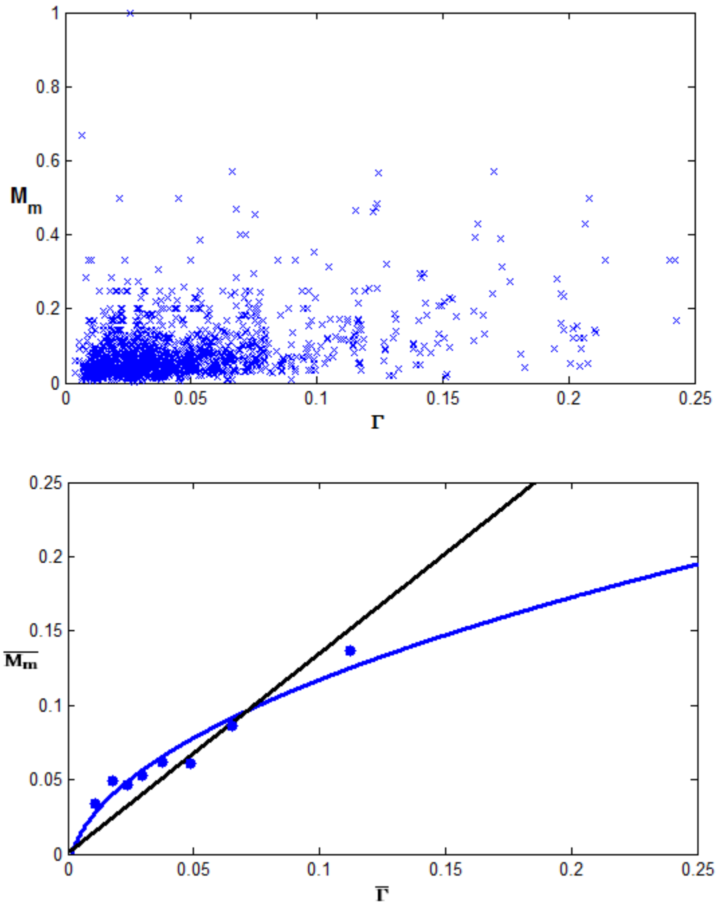


**Figure 4.13** Raw data and average behavior of mixed marriages quantifier in period 1.

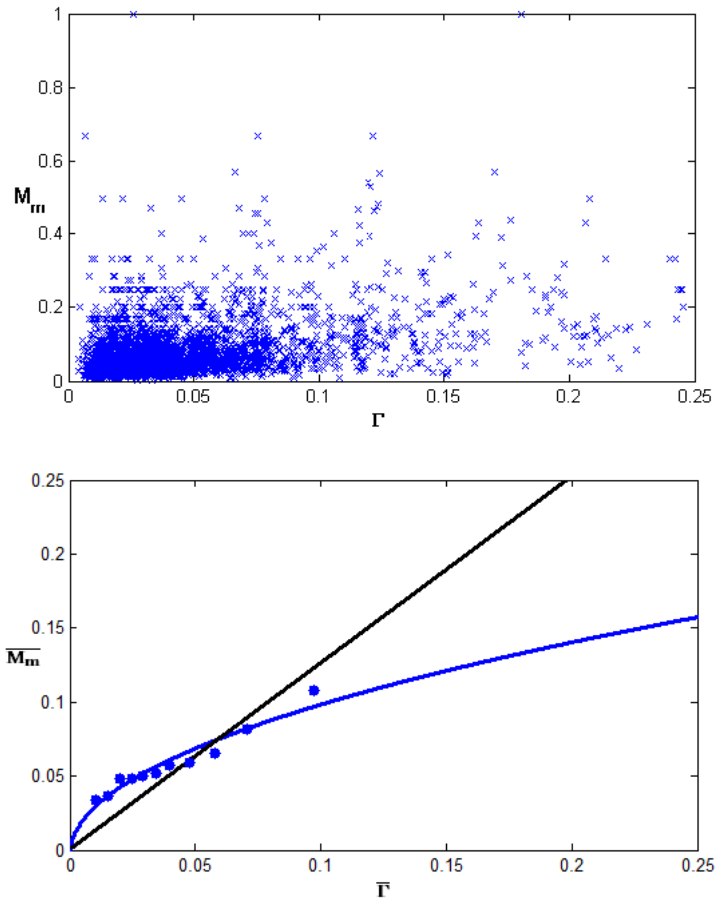


**Figure 4.14** Raw data and average behavior of mixed marriages quantifier in period 2.

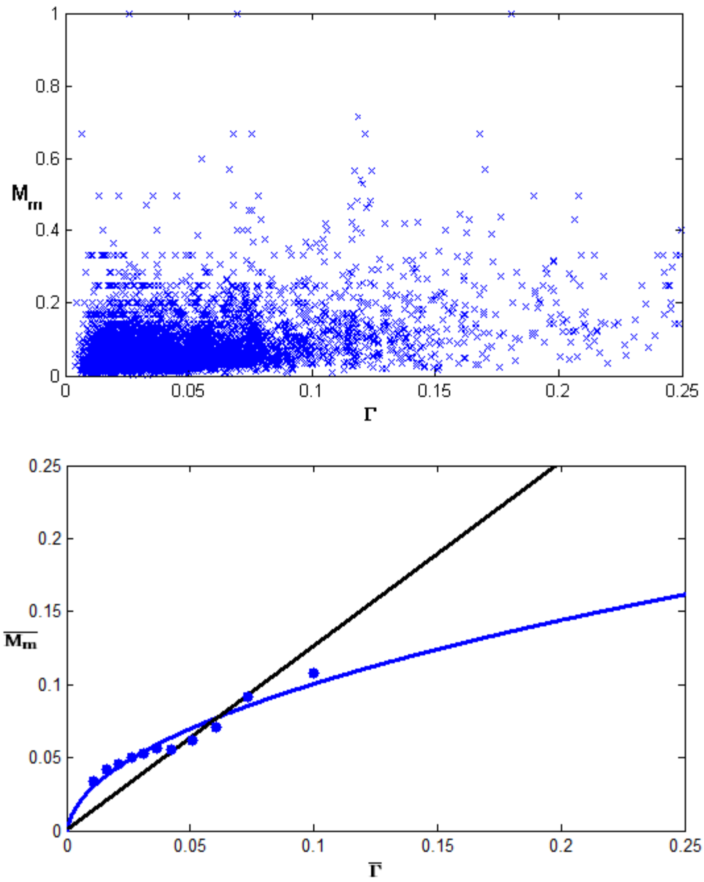


**Figure 4.15** Raw data and average behavior of mixed marriages quantifier in period 3.

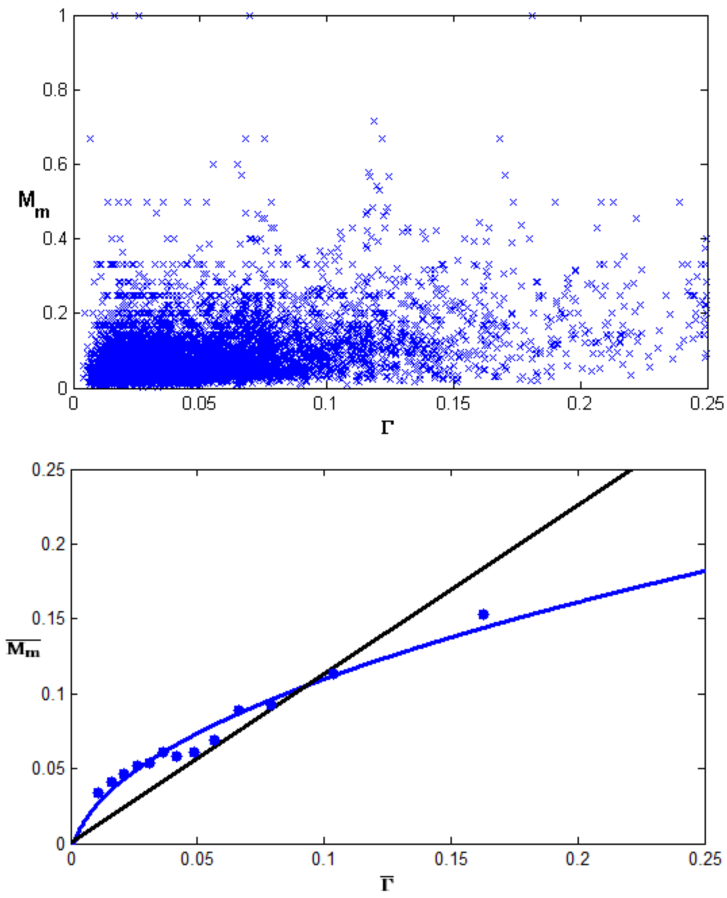


**Figure 4.16** Raw data and average behavior of mixed marriages quantifier in period 4.

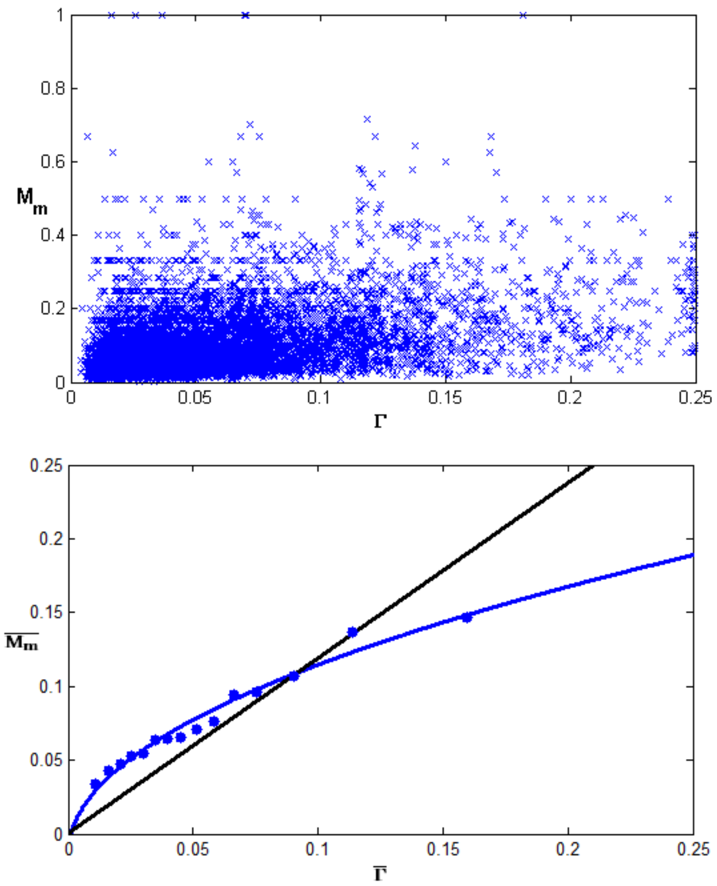


**Figure 4.17** Raw data and average behavior of mixed marriages quantifier in period 5.

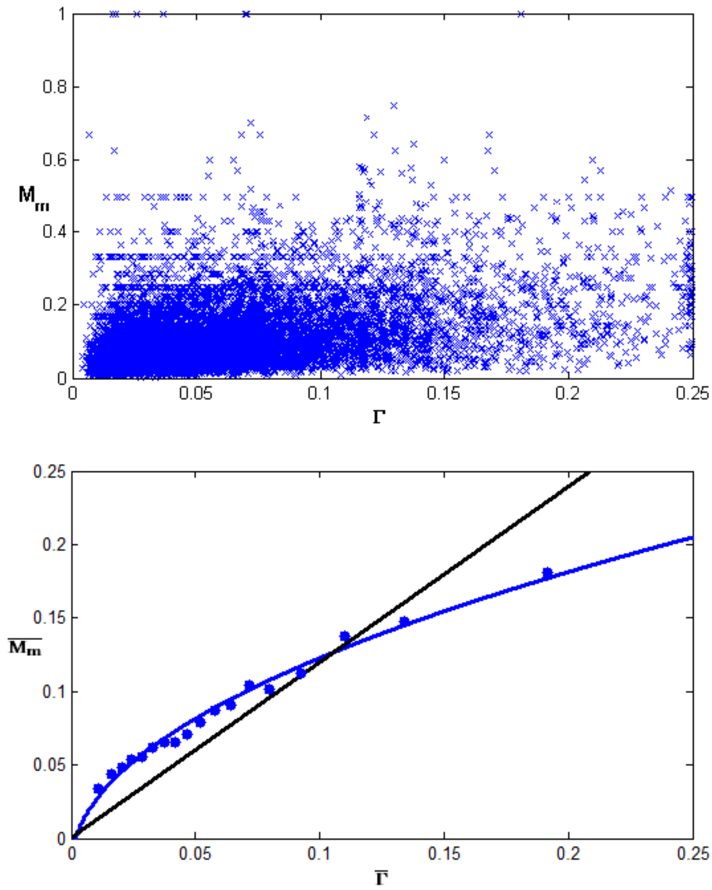


**Figure 4.18** Raw data and average behavior of mixed marriages quantifier in period 6.

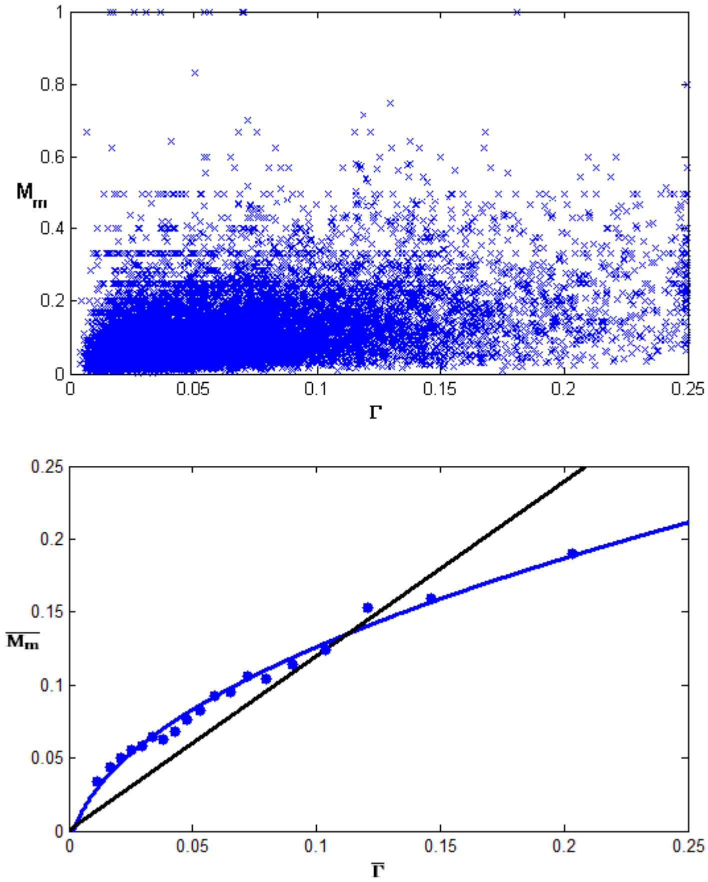


**Figure 4.19** Raw data and average behavior of mixed marriages quantifier in period 7.

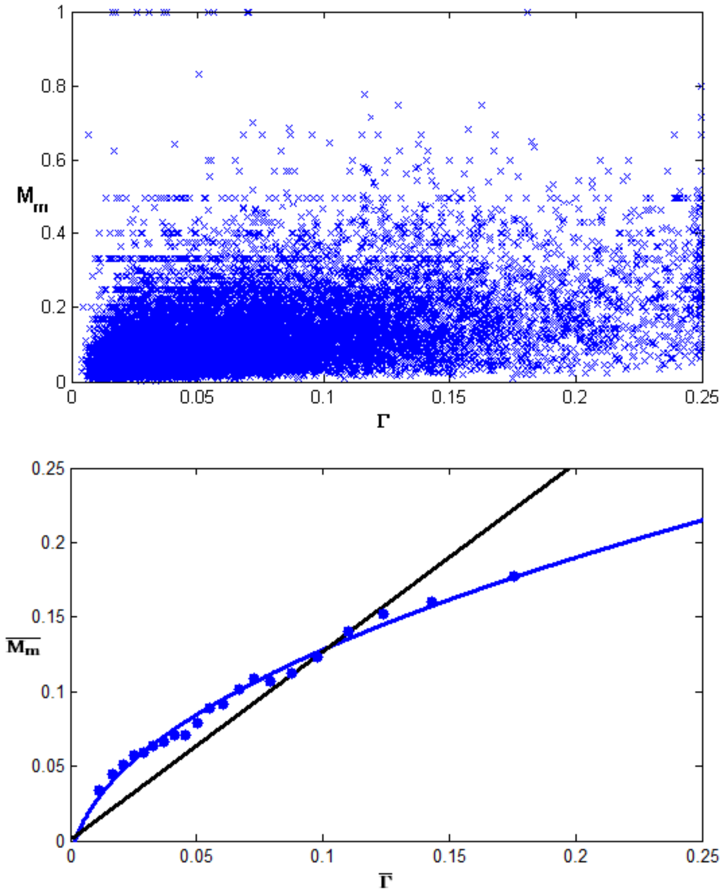


**Figure 4.20** Raw data and average behavior of mixed marriages quantifier in period 8.

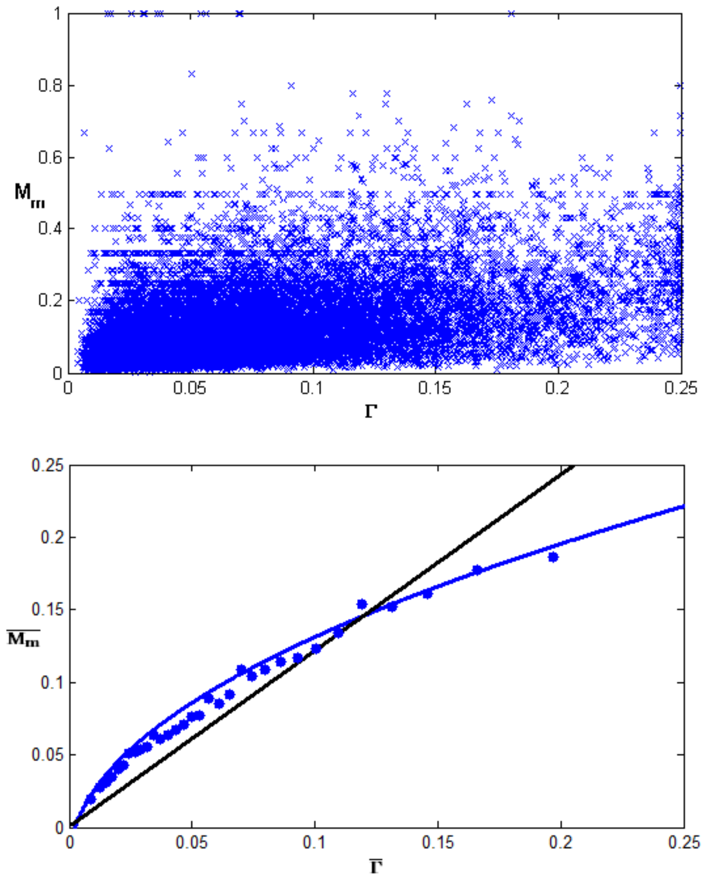


**Figure 4.21** Raw data and average behavior of mixed marriages quantifier in period 9.

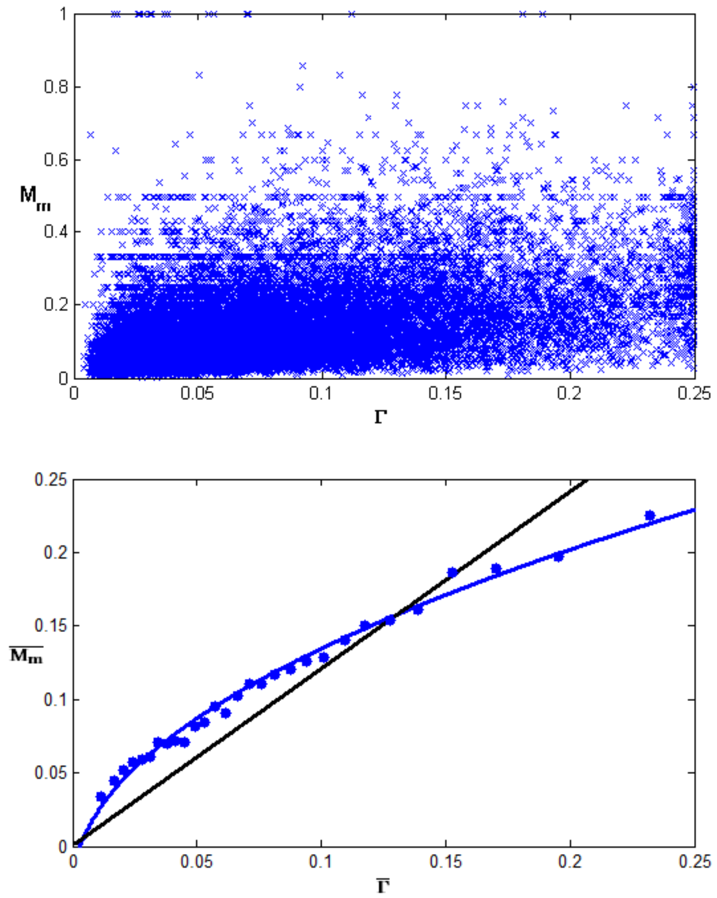


**Figure 4.22** Raw data and average behavior of mixed marriages quantifier in period 10.

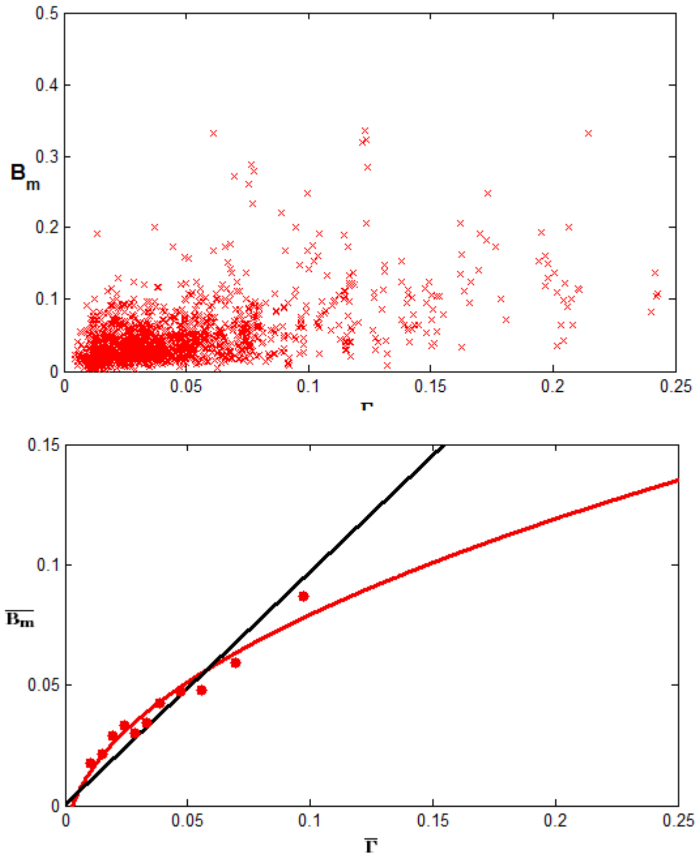


**Figure 4.23** Raw data and average behavior of newborns quantifier in period 1.

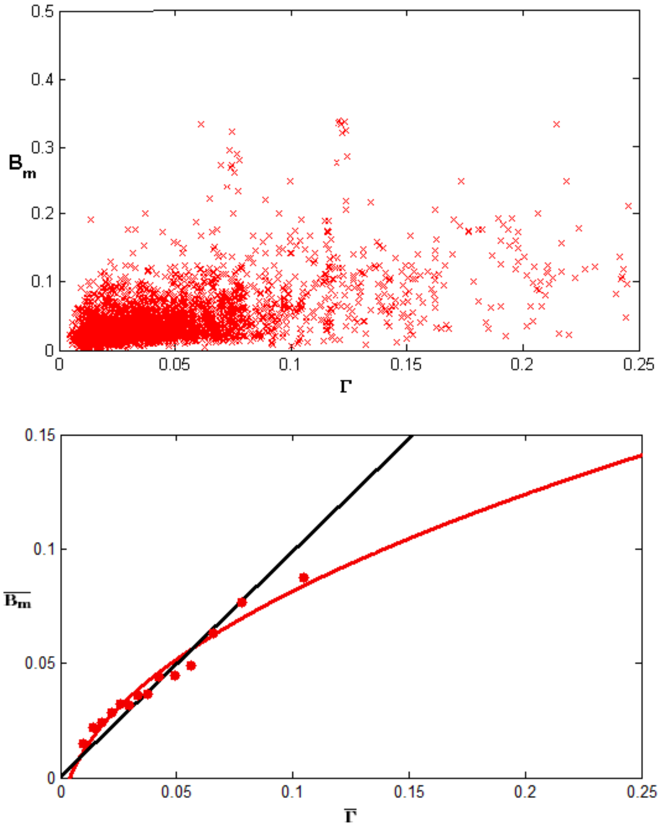


**Figure 4.24** Raw data and average behavior of newborns quantifier in period 2.

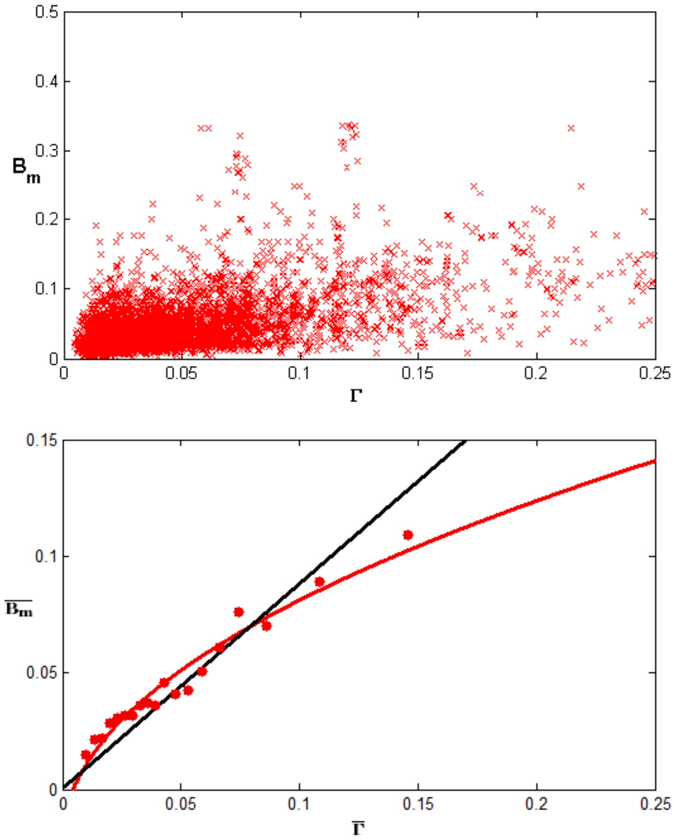


**Figure 4.25** Raw data and average behavior of newborns quantifier in period 3.

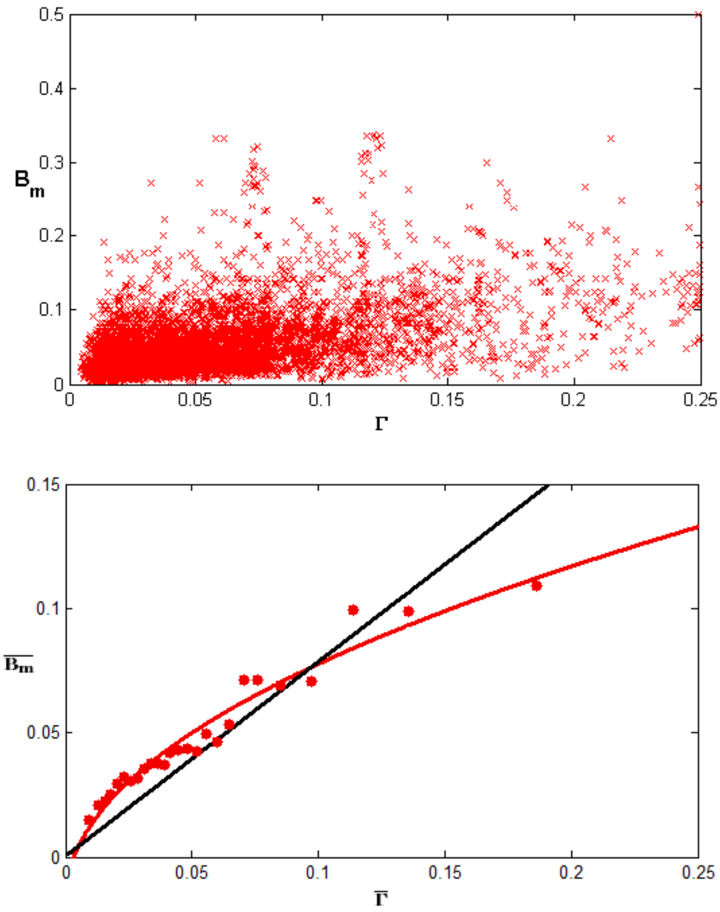


**Figure 4.26** Raw data and average behavior of newborns quantifier in period 4.

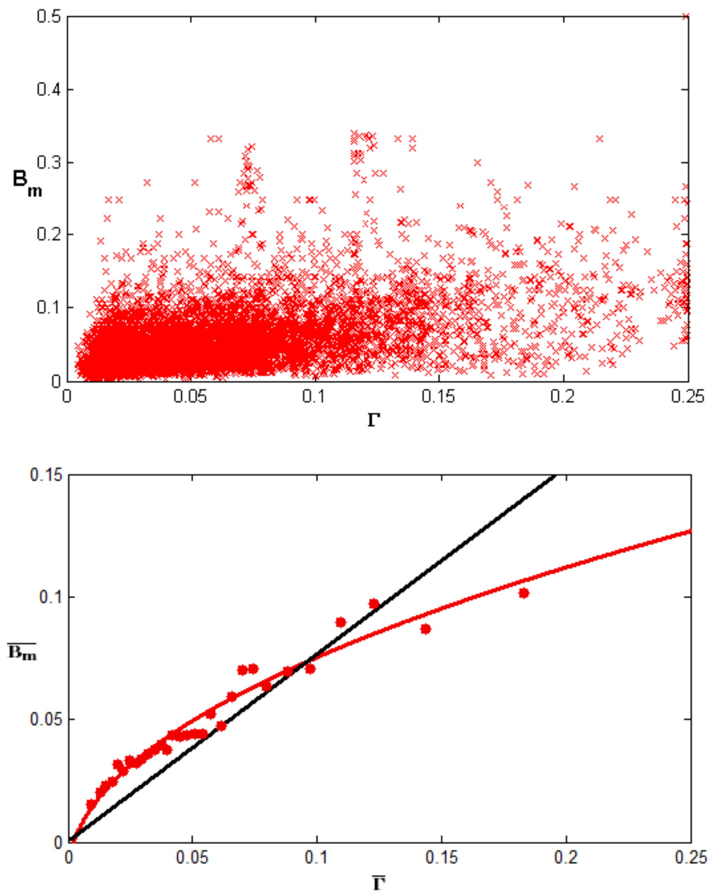


**Figure 4.27** Raw data and average behavior of newborns quantifier in period 5.

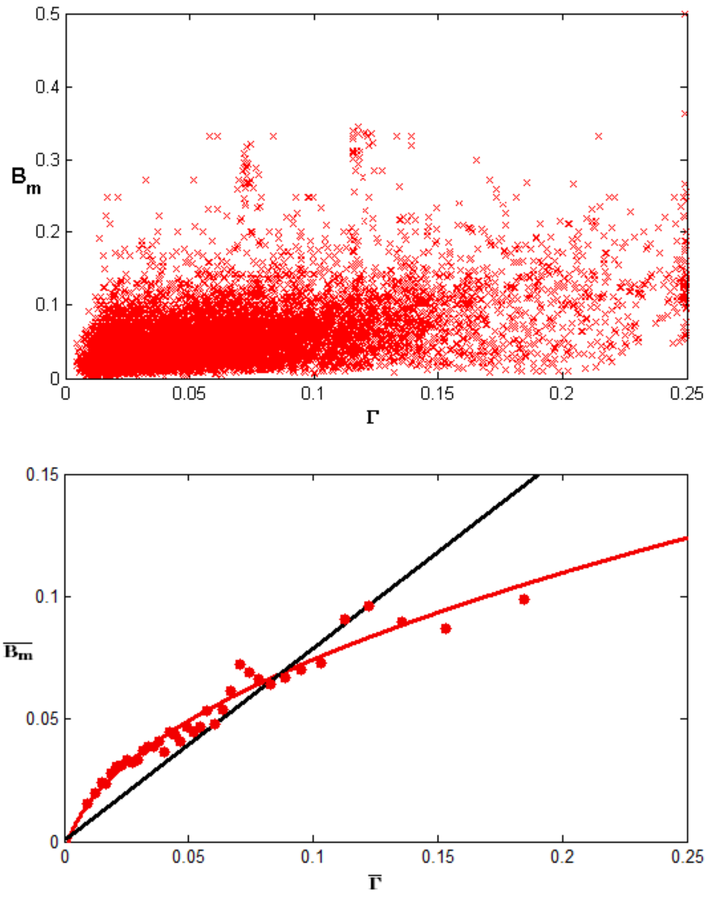


**Figure 4.28** Raw data and average behavior of newborns quantifier in period 6.

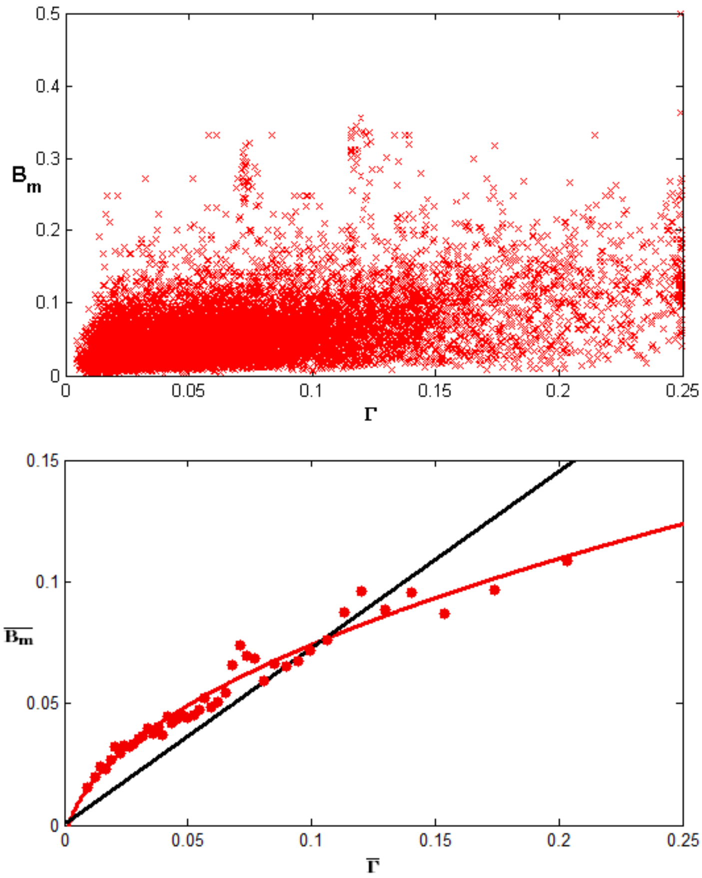


**Figure 4.29** Raw data and average behavior of newborns quantifier in period 7.

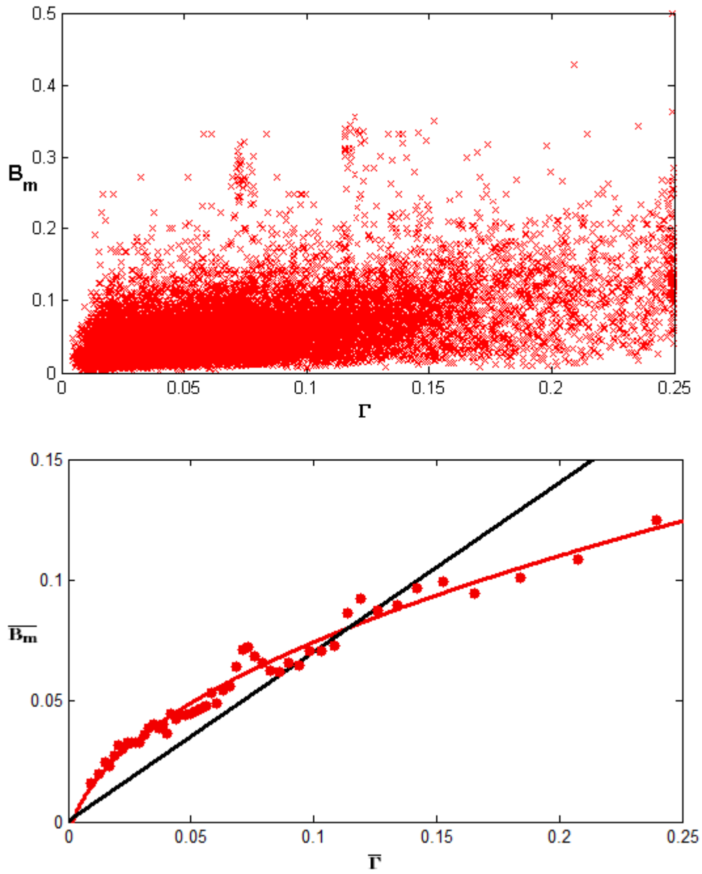


**Figure 4.30** Raw data and average behavior of newborns quantifier in period 8.

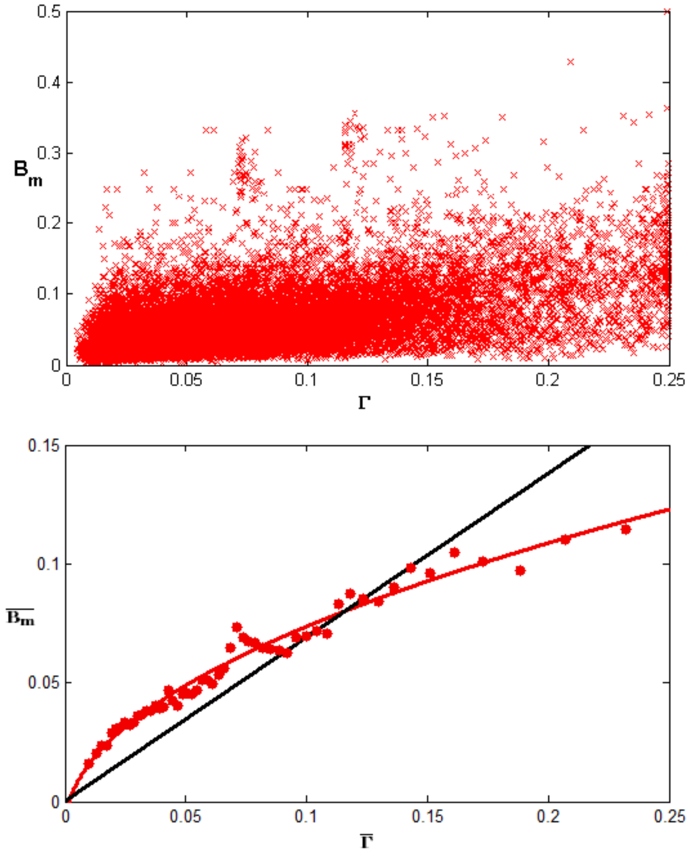


**Figure 4.31** Raw data and average behavior of newborns quantifier in period 9.

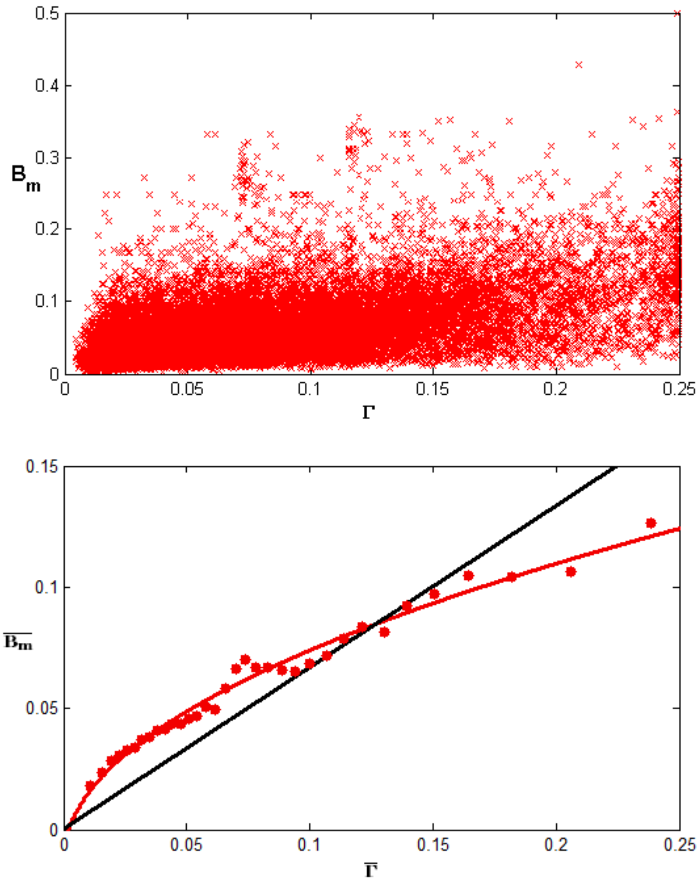


**Figure 4.32** Raw data and average behavior of newborns quantifier in period 10.